REVIEW ARTICLE

CrossMark

Continuous magnetic droplets and microfluidics: generation, manipulation, synthesis and detection

Entesar Al-Hetlani[1] (ID) · Mohamed O. Amin[1]

Abstract

In this review, an introduction is given to provide the fundamental principles of magnetic droplet microfluidics. This is followed by a thorough discussion of methods that have been developed for the continuous generation of magnetic droplets and their controlled and precise manipulation by using external magnetic fields. Next, attention is given to techniques devised for the continuous fabrication of magnetic materials in droplets with an emphasis on the synthesis and modification of magnetic nanoparticles (MNPs), magnetic microstructures, Janus microparticles and magnetic hydrogels. In addition, selected applications of continuous magnetic droplets in (bio)assays and detection methods are discussed. The review (with 113 refs.) ends with concluding remarks and a discussion of current challenges and the future outlook for the field of continuous magnetic droplet microfluidics.

Abbreviations

aMWCNTs	Acidified multi wall carbon nanotubes
a.u.	Arbitrary unit
BacNWs	Bacterial magnetic nanowires
B_o	Bond number
BSA	Bovine serum albumin
BET	Brunauer-Emmett-Teller
Ca	Capillary number
CMC	Carboxymethyl cellulose
CH	Congenital hypothyroidism
CV	Coefficient deviation/ Coefficient of variance
CUR	Curcumin
DSC	Differential scanning calorimetry
DMF	Digital microfluidics
DMMF	Droplet micro-magnetofluidics
EWOD	Electrowetting on dielectric
C_{max}	Entrance of the throat
ETFE	Ethylene tetrafluoroethylene
ETPTA	Ethoxylated trimethylolopropane triacrylate
FR	False rate of counting
FF	Ferrofluid
FEM	Finite element method
FTIC-BSA	Flourescein isothiocyanate-bovine serum albumin
5FU	5 fluorouracil
Q_d	Flow rate of the dispersed phase
Q_c	Flow rate of the continuous phase
Q_i	Flow rate of the inner phase
Q_o	Flow rate of the outer phase
FTIR	Fourier-transform infrared spectroscopy
FFM	Free-flow magnetophoresis
GA	Glutaraldehyde
GMR	Giant magnetoresistive
GO	Graphene oxide
HSA	Human serum albumin
HSA-MB	Human serum albumin-magnetic beads
HCPK	1-hydroxycyclohexyl phenyl ketone
IFD	Initial ferrofluid droplet
FFD	Final ferrofluid droplet
F_i	Interfacial tension force
KHz	KiloHertz
LbL	Layer-by-layer

✉ Entesar Al-Hetlani
Entesar.alhetlani@ku.edu.kw

✉ Mohamed O. Amin
Mohamed.amin@ku.edu.kw

[1] Faculty of Science, Department of Chemistry, Kuwait University, P.O. Box: 5969, 13060 Kuwait City, Kuwait

K_L	Lift force ratio
K_M	Magnetic force ratio
x_m^*	Magnet location
MNPs	Magnetic nanoparticles
MP	Magnetic polymeric phase
MGITC-AuNPs	Malachite green isothiocyanate gold nanoparticles
L_{mig}^*	Migration length
MPGCBs	Magnetic porous graphene oxide/multi-walled carbon nanotube beads
NPs	Nanoparticles
NIR	Near infrared
Nd-Fe-B	Neodymium-iron-boron
MOPS	3-(N-Morpholino)propanesulfonic acid
$F_{R,net}$	Net force
NB	Non-breakup
F_l	Non-inertial lift force
NM	No magnetic field
Oe	Oersted
O/W	Oil-in-water
MIL	Paramagnetic ionic liquid
P	Penicillin
BPO	Permanent obstruction
PDMS	Polydimethylsiloxane
PFA	Perfluoroalkoxy alkane
PEGDA	Poly(ethylene glycol) diacrylate
PEG-PFPE	Polyethylene glycol perfluoropolyether
PEDOT/PSS	Poly(3,4-ethylenedioxythiophene)/ polystyrene sulfonate
PE	Polyelectrolytes
PEEK	Polyether ether ketone
PAH-FTIC	Poly(fluorescein isothiocyanate allylamine hydrochloride)
PP	Polymeric phase
PCR	Polymerase chain reaction
PLL	Poly(L-lactic acid)
PS	Polystyrene
PSS	Poly(sodium-4-styrerne sulfonate)
PTFE	Polytetrafluoroethylene
PVA	Polyvinyl alcohol
P(VDF-TrFE)	Poly(vinylidene fluoride-trifluoroethylene)
PVP	Polyvinylpyrrolidone
QDs	Quantum dots
Re	Reynolds number
RITC	Rhodamine B isothiocyanate
M_s	Saturation magnetization
SEM	Scanning electron microscopy
SEM-EDX	Scanning electron microscopy-energy dispersive X-ray spectroscopy
SiNPs	Silicon nanoparticles
SDS	Sodium dodecyl sulfate
SAR	Specific absorption rates

SERS	Surface enhanced Raman spectroscopy
SDA	Supervised discriminant analysis
BTO	Temporary obstruction
THF	Tetrahydrofuran
TGA	Thermogravemtric analysis
TPGDA	Tri(propylene glycol) diacrylate
UM	Uniform magnetic field
W/O/W	Water-in-oil-in-water droplets
We	Weber number
VSM	Vibrating sample magnetometer
BNO	Without obstruction
XPS	X-ray photon spectroscopy
XRD	X-ray powder diffraction

Symbols

g	Acceleration of gravity
θ	Angle
C	Concentration
l	Characteristic length scale
cP	Centipoise
$\Delta\rho$	Difference in density
$\Delta\chi$	Difference in magnetic susceptibility
F_d	Drag force
η	Dynamic viscosity
γ	Interfacial tension
∇B	Magnetic field gradient
H	Magnetic field strength
B	Magnetic flux density
F_{mag}	Magnetic force
M	Magnetization
μm	Micrometer
μL	Microlitres
μV	Microvolts
mPa	Milli Pascal
mT	Milli Tesla
nN	Nanonewtons
N	Number of MNPs
μ_0	Permeability of vacuum
pL	Picolitres
pN	Piconewtons
r	Radius of the droplet
σ	Standard deviation
v	Velocity
u_{defl}	Dragged velocity
u_{hyd}	Hydrodynamic flow velocity
u_{mag}	Magnetic velocity
V	Volume

Introduction

A sub-branch of the field of microfluidics, the science of manipulating and controlling fluids, focuses on multiphase

systems containing droplets. Droplet microfluidic systems have significant advantages over their single-phase counterparts and, as a result, they become attractive and versatile alternatives for several key applications [1]. Droplets are spheres or plugs of fluid dispersed in other immiscible fluids (or simply air), where all or parts of the channel are blocked without actually being in direct contact with the channel walls [2, 3]. Typically, droplets are referred to as the dispersed phase (inner phase) in a surrounding continuous carrier phase (outer phase). Droplets have incredibly small volumes that range from picolitres (pL) to microlitres (μL), and dimensions usually in the micrometer (μm) range. [3]. Continuous generation at high frequencies (ca. tens of KiloHertz, KHz) enables the production of more than 500 monodispersed droplets per second with size coefficient deviations (CV) of less than 2% [4]. While over the past two decades, droplet microfluidic systems have been extensively utilized by many research groups to study protein crystallization [5], optimize screening conditions [6] and detect bacteria [7].

Compared to conventional methods, microfluidic devices are capable of producing large quantities of monodispersed droplets [8]. As a result, use of these droplets for screening processes are both cost-effective and significantly less time consuming. In addition, rapid mixing to homogenize reagents within droplets can be achieved by using two mechanisms including diffusion and chaotic advection [9]. Heat transfer and dissipation, critical for the success of processes such as the polymerase chain reaction (PCR), can be highly controlled in small droplets owing to their high surface area-to-volume ratio [10]. Droplets are surrounded by an inert and immiscible fluid layer that isolates them from channel walls, thus, eliminating cross-contamination of contents between droplets and preventing droplet evaporation [6, 11]. Furthermore, manipulation of droplets inside microchannels requires minimal force. The force on a small amount of liquid in a microfluidic channel can be determined using the Stokes' drag (F_d in N) equation (Eq. 1),

$$F_d = 6\pi\eta r v \tag{1}$$

where η is the dynamic viscosity of the continuous phase (in kg m^{-1} s^{-1}), r is the radius of the droplet (in m) and v is the droplet velocity (in m s^{-1}). Since the values of r and v are small the force exerted on the droplet is estimated to be in the range of tens nanonewtons (nN) to piconewtons (pN) [12], which can be easily achieved for example by using magnetic fields.

A number of dimensionless values such as the Reynolds number (Re), Weber number (We), Bond number (B$_o$) and capillary number (Ca) are commonly employed to describe the behavior of fluids in the microscale [13]. Among these, B$_o$ and Ca are significant to describe the influence of physical forces on droplets formation and stability within the microchannels. B$_o$ relates the effect of gravitational force on interfacial tension through Eq. 2,

$$B_o = \frac{\Delta\rho g l^2}{\gamma} \tag{2}$$

where $\Delta\rho$ is the difference between the densities of the dispersed and continuous phases (Kg m^{-3}), g is the acceleration of gravity (m s^{-2}), l is a characteristic length scale (m) and γ is the interfacial tension (N m^{-1}). In droplet microfluidics, B$_o$ is preferably maintained below unity (B$_o$ << 1) so that the effect of gravitational force is negligible.

In contrast, Ca relates the interfacial tension to viscosity through Eq. 3

$$Ca\frac{\eta v}{\gamma} \tag{3}$$

where η is the viscosity of the most viscous phase (Kg m^{-1} s^{-1}) and v is the velocity of that phase (m s^{-1}). When Ca is much less than unity, interfacial forces dominate and, consequently, spherical droplets are normally formed as a result of surface area minimization. On the other hand, when Ca is much larger than unity (Ca >> 1), deformed and asymmetrical droplets are produced because of the dominance of viscous forces [14].

Introduction to magnetic droplets

A methods for continuous generation and handling of discrete magnetic liquids within microfluidic channels was first developed in 2004 by Pekas et al. [15]. The protocol was uniquely applied to monitor the velocity and size of moving magnetic droplets. A magnetic droplet is defined as a small volume of liquid that possesses a magnetic core and responds to an external magnetic field. Introduction of magnetic functionality into a droplet was achieved by incorporating a ferrofluid (FF) comprised of magnetic nanoparticles (MNPs) or microparticles (sometimes referred to as beads) into the dispersed phase. FFs are suspensions of MNPs, which have typical dimensions of approximately 10 nm. These particles possess superparamagnetic properties and are normally coated with a surfactant or charge in order to give them stability in the carrier liquid [16]. FFs are either water or oil based and are commercially available with a range of magnetic properties from companies such as *Ferrotec* (www.ferrotec.co.uk) [17, 18]. On the other hand, magnetic microparticles composed of iron oxide nanoparticles (NPs) embedded in polymeric or a silica shell in the μm range are commercially available (for example from www.invitrogen.com) and can be suspended in liquids to produce magnetic droplets [19].

Magnetic components are incorporated into droplets to promote actuation, prepare novel magnetic materials and/or

perform bio-analysis process. Microfluidic platforms used to generate magnetic droplets range from simple capillary assemblies to more complex setups incorporating connected sealed microdevices comprised of different substrates. Tables 1, 2, 3, and 4 contain overviews of the various types of substrates, with methods for surface modification, magnetic materials, continuous phase and surfactants used to produce magnetic droplets. Moreover, Table 5 lists the common types of substrates used in the fabrication of microfluidic devices for magnetic droplet generation and their advantages and disadvantages.

The term micro-magnetofluidics has been utilized in the current literature to describe platforms which combine magnetism and microfluidics [20]. Although this term is not new, it has been used recently for systems which employ magnetic fluids for sensing and actuation purposes. More broadly, this term refers to devices in which flowing magnetic fluids on the microscale are used for actuation, manipulation and detection applications. This topic has been covered in a detailed review recently prepared by Nam-Trung Nguyen [20].

Unlike nonmagnetic droplets, which require relatively complex methods for manipulation [21, 22], their magnetic analogs have several advantageous features when generated in microfluidic devices. For example, introducing magnetic control directly into droplet microfluidics can be simply accomplished and actuation of the droplets does not require integrated mechanical components such as pumps and valves or special channel designs [23]. Moreover, magnetic droplets are relatively insensitive to changes in pH, ionic strengths and surface charge [24]. Actuation of these droplets can be affected by temperature, viscosity and the magnetic properties of the magnetic moiety [25]. The key parameters that influence the behavior of magnetic droplets subjected to magnetic fields are their volume, the difference between the magnetic susceptibility of the droplet and surrounding medium and the strength and gradient of the applied magnetic field [24]. Thus, The magnetic force acting on magnetic droplets, (F_{mag}, in N), is defined in Eq. 4:

$$F_{mag} = \frac{\Delta\chi\,V\,N}{2\mu_0}\,\nabla B^2 \qquad (4)$$

where $\Delta\chi$ is the difference in magnetic susceptibility between the magnetic droplet and the carrier phase (dimensionless), V is the volume of the droplet (in m^3), N is the number of magnetic particles in each droplet (dimensionless), B is the magnetic flux density (in T), ∇B is the magnetic field gradient (in T m^{-1}) and μ_0 is the permeability of vacuum ($4\pi \times 10^{-7}$ H m^{-1}) [25]. Therefore, by selecting ∇B and $\Delta\chi$ the magnetic force on the droplet can be controlled.

A moving magnetic droplet (or bead) in a magnetic field experiences an equal but opposing force due to the influence

Table 1 An overview on capillaries/chips made from glass and fused silica, with methods for surface modification, magnetic materials, continuous phase and surfactants used to generate magnetic droplets

Chip/capillary material	Surface modification	Dispersed phase (magnetic material)	Continuous phase	Surfactant	Ref.
Glass capillaries	Hydrophobized (reagent not specified)	MIL [bmin]FeCl₄	Silicone oil	–	[29]
Glass capillaries	–	FF (EMG 905)	Water	SDS (1%, w/w)	[69]
Glass capillaries	–	9.1 ±2.7 nm functionalized MNPs	Glycerol (64 wt%), PVA (2 wt%) and water (34 wt%)	SDS	[78]
Glass capillaries	–	15 nm NiZn ferrite MNPs, GO and water	diluted silicone oil, amodimethicone (KF-860) and diamino-modified polymeric silicone	–	[89]
Glass capillaries	–	12 nm Fe₃O₄ NPs and 200–300 nm SiO₂ NPs	Silicone oil	–	[91]
Glass chip	–	FF (EMG 901)	PSS and PAH-FITC	SDS solution (1% w/v), Tween 20 (0.5% v/v) and Tween 60 (0.05% v/v)	[57]
Glass chip	Trichloro(perfluoroooctyl)silane	FF (EMG 507)	Perfluorodecalin	1H,1H,2H,2H-perfluoro-1-octanol (10% v/v)	[18]
Glass chip	–	FF (EMG 705) Polyethylene oxide nitrodopaime coated Fe₃O₄ NPs	PVA aqueous solution (2% wt/v%)	–	[84]
Fused silica capillaries	1H,1H,2H-perfluorooctyltriethoxysilane	2.8 μm magnetic beads and 8–15 μm Fe₃O₄ ferromagnetic particles	n-tetradecane	Span 80 (2%)	[98]

Table 2 An overview on capillaries/tubings made from fluorinated materials, with methods for surface modification, magnetic materials, continuous phase and surfactants used to generate magnetic droplets

Chip/capillary material	Channel modification	Dispersed phase	Continuous phase	Surfactant	Ref.
PTFE capillaries	–	9 ± 0.22 nm γ-Fe$_2$O$_3$	FC-40	1H,1H,2H,2H-perfluorodecan-1-ol (2 wt%)	[81]
PTFE pipes	–	Fe$_3$O$_4$/PS	Two continuous phases (1) ETPTA and initiator (2) water	PVA (4%)	[82]
Fluorinated ethylene propylene capillaries	–	FF (EMG 507), PEGDA, PPS and HMP	Hexane	–	[79]
Teflon tubing	–	1 μm streptavidin coated magnetic beads	FC-40	1H,1H,2H,2H-perfluorodecan-1-ol (0.1 to 3%)	[100]
Teflon tubing	–	130 μm magnetic particles	FC-40	1H,1H,2H,2H-perfluoro-1-octanol (3%)	[41]
PFA capillary tubing	–	EMG 807	Heavy mineral oil Silicone oil	–	[53]

of the hydrodynamic flow. Under this condition, the sum of F_{mag} and F_{drag} (Eq. 5) equals zero [26]:

$$F_{mag} + F_{drag} = 0 \qquad (5)$$

therefore, the velocity of the magnetic droplet can be calculated by using Eq. 6, which arises by combining Eqs. 1, 4 and 5.

$$v = \frac{\Delta\chi \, V \, N}{12 \, \pi \, r \, \eta \, \mu_0} \nabla B^2 \qquad (6)$$

The methods employed to generate non-magnetic and magnetic droplets are similar, typically incorporating T-junction [27], flow focusing configurations [28], capillary/tubing assembly [29], pipetting [30], electrowetting on dielectric (EWOD) [31] or less common designs such as electrospray devices [32]. The term "digital microfluidics" (DMF) is often used in the literature to denote the manipulation of discrete and relatively large volumes (ca. μL) of liquids on a surface using various mechanisms, such as EWOD [33], dielectrophoresis (DEP) [34], thermocapillary transport [35], electromagnetic pillar arrays [36], and surface acoustic waves (SAWs) [37]. DMF refers to techniques for microscale electrostatic fluid-handling that enables the control of discrete droplets on an electrode array and, as a result, it is beyond the scope of this review.

Key processes, including transporting, merging, splitting, mixing, sorting and detecting magnetic droplets, can be accomplished in microfluidic platforms using several interesting approaches [38]. For example, several publications by Nguyen and his co-authors have focused on the formation and manipulation of magnetic droplets in microfluidic systems [27, 39, 40]. In several of the approaches, surfactants were added to the dispersed or the carrier phase to reduce interfacial tension between the two phases, which facilitates

droplet formation and stability. In other techniques, surfactants were used to assist droplet splitting [41] or to reduce magnetic bead aggregation, which would lead to a decrease in the available surface for binding [42]. Baret prepared a detailed review discussing the roles surfactants play in droplet microfluidics [43].

Thus far, several reviews have appeared covering recent advances made in the generation, maneuvering and application of droplet micorfluidics [44, 45]. Additionally, numerous reviews have focused on the utilization of magnetic particles in single-phase microfluidic devices including those that discuss microfluidics and magnetism [24] for bio-analysis [46], catalysis [47] and micromixers [48], and the interactions occurring between magnetism and fluid flow on the microscale [20]. Furthermore, the integration of droplet microfluidics and magnetism was the focus of one review dedicated to DMF [49]. However, a survey of the literature shows that no reviews have been published that discuss the growing number of applications of continuous magnetic droplets in microfluidics. Thus, this review fills that gap by providing a detailed overview of studies carried out on continuous magnetic droplets within sealed microfluidic systems. The review is divided into five sections that discuss (1) magnetic droplet generation, (2) magnetic droplet manipulation, (3) synthesis of magnetic materials, (4) assay-based magnetic droplets and (5) magnetic droplet detection.

Continuous magnetic droplet generation

Generation of droplets having uniform sizes and distributions is one of the most important advantages of microfluidics. Since the time of their discovery, droplets

Table 3   An overview on chips made from PDMS, with methods for surface modification, magnetic materials, continuous phase and surfactants used to generate magnetic droplets

Chip/capillary material	Channel modification	Dispersed phase	Continuous phase	Surfactant	Ref.
PDMS chip	–	FF (EMG 507)	Perfluorodecalin	Tridecafluorooctanol (10% v/v)	[15]
PDMS chip	–	1 μm amine terminated magnetic beads	Mineral oil	Span 80 (4% w/w)	[19]
PDMS chip	–	FF (EMG 807)	Silicone oil	–	[27]
PDMS chip	–	FF (EMG 408)	Novec 7500 and FC-40 (fluorinated oil)	Pico-Surf 1	[54]
PDMS chip	–	16 nm Fe_3O_4 NPs	Dimethylsilicon oil	–	[59]
PDMS chip	–	10 ± 2 nm Fe_3O_4 NPs	Mineral oil	–	[60]
PDMS chip	–	FF (MF01)	Water	–	[61]
PDMS chip	–	FF (EMG 807)	Silicone oil	–	[39, 40]
PDMS chip	–	FF (fluidMAG-PAS)	Mineral oil	Span 80 (5%)	[74]
PDMS chip	–	Fe_3O_4 NPs	Plant oil	–	[52]
PDMS chip	–	1 μm magnetic beads	FC-40	PEG-Di-Krytox (2% w/w)	[75]
PDMS chip	Aquapel	$FeCl_2.4H_2O$ and $FeCl_3.6H_2O$	FC-40	Ammonium salt of a PFPE (2.5% wt/wt)	[77]
PDMS chip	–	8.1 nm oleic acid coated MNPs	Water	–	[107]
PDMS chip	–	$FeSO_4 \cdot 7H_2O$, $MnCl_2 \cdot 4H_2O$ and _E. coli_ cells	FC-40	PEG-PFPE	[80]
PDMS chip	–	Fe_3O_4 NPs, PEDOT/PSS and PVA	Silicone oil	DC 5225	[88]
PDMS chip	–	PEGDA, water, and FF with Darocur and Irgacure 819 photoinitiators	Light mineral oil	ABIL EM 90 (3% v/v)	[95]
PDMS chip	–	QD and Fe_3O_4 NPs in queous alginate	$CaCl_2$ and oleic acid	–	[93]
PDMS chip	–	200 nm Fe_3O_4 NPs and P(VDF-TrFE) powders in dimethylformamide	Mineral oil	Span 80 (2% wt%)	[94]
PDMS chip	Aquapel, 47,100	2.8 μm magnetic beads	Mineral oil (M8410)	Span 80 (2%)	[26]
PDMS chip	–	50 nm Fe_3O_4 NPs	Mineral oil	Span 80 (2%)	[101]
PDMS chip	Trichloro(1H,1H,2H,2H -perfluorooctyl) silane	1 μm magnetic beads	FC-40 and FC-70	1H,1H,2H,2H-perfluorodecan-1-ol	[97]
PDMS chip	Tetraethoxysilane	FF (EFH Series-oil-based)	50% Aqueous solution of PEG	SDS (1%)	[105]
PDMS chip	–	FF (EMG 700)	M8410 mineral oil	Span 80 (5%)	[106]
PDMS chip	–	EMG 408	Silicone oil AP1000 and mineral oil	Glycerol	[63]

have been generated mainly by using pressure [18], electric [50] and centrifugal forces [51]. The use of magnetic forces alone or in combination with others to generate monodispersed droplets has emerged as a new tool to control the sizes, magnetic contents and frequencies of generated droplets.

Tan et al. [27] demonstrated that FF droplets can be generated at a T-junction (Fig. 1a) in the absence and presence of a permanent magnetic field. In the absence of a magnetic field, the size of the droplets decreased as the flow rate of the continuous phase (Q_c) is increased and the size of the FF droplets decreased as the capillary number (Ca) is increased (Fig. 1b). However, in the presence of a magnetic field, the size of the droplets depended on the factors affecting magnetic force including the magnetic field strength (B) and gradient (∇B), and the magnetization of the FF (M). At fixed dispersed flow rates (Q_d) and Q_c, when the magnetic field was positioned upstream from the droplet generation point, the droplet size increased as B increased. In contrast, when the field was located downstream, the droplet size decreased as B increased. These phenomena are a consequence of the effect of the magnetic force on the droplet as it emerges at the T-junction, which retarded its movement and delayed the breakup process. Furthermore, increasing both B and Q_c led to the production of smaller magnetic droplets. The influence of a uniform magnetic field on the generation of FF droplets in a flow focusing configuration rather than a T-junction has been elucidated [39, 40].

Table 4　An overview on capillaries/chips made from various other materials (such as PMMA, hybrid materials and composites), with methods for surface modification, magnetic materials, continuous phase and surfactants used to generate magnetic droplets

Chip/capillary material	Channel modification	Dispersed phase	Continuous phase	Surfactant	Ref.
PMMA chip	–	FF (EMG 807)	Mineral oil	Span 20 (4%, w/w)	[64]
PMMA chip	–	FF (EMG 807)	Mineral oil	Span 20 (4% w/w)	[66]
PMMA chip	–	FF (EMG 807)	Silicone oil	Tween 20 (0.3% v/v)	[76]
PMMA chip	–	γ-Fe$_2$O$_3$ NPs and chitosan in water	Hexadecane	Span 80 (2%, w/w)	[83]
PMMA chip	–	FeCl$_2$.4H$_2$O, FeCl$_3$.6H$_2$O and chitosan	Sun flower seed oil	–	[85]
PDMS/glass chip	Parts were grafted with polyacrylic acid	FF (EFH1)	HFE-7500 (fluorinated oil)	Krytox 157FSL	[28]
PDMS/glass chip	(heptadecafluoro-1,1,2,2-tetrahydrodecyl) trichlorosilane	1 μm magnetic beads	HFE7500 fluorinated oil	PEG-Krytox surfactant	[44]
PDMS/Ni microstructure chip	–	56 nm neutral dextran-coated MNPs	Mineral oil	–	[62]
Glass capillaries and PTFE tubing	–	50 nm MNPs, TPGDA, HCPK and (methacryloxypropyl) methyl siloxane–dimethylsiloxane copolymer	Sodium carboxymethyl cellulose and water	–	[92]

A magnetic tweezers based approach for continuous magnetic droplet generation and manipulation was also developed by Yan et al. [52]. In this technique, Fe$_3$O$_4$ NPs were prepared off-chip using a solvothermal method and characterized using TEM and by analyzing a magnetization curve which showed that they are superparamagnetic. Using a flow-focusing geometry, the FF, comprised of a deioinzed water dispersion of the NPs, was fed and merged with the continuous phase to form magnetic droplets. The microfluidic device was placed in the gap between the middle of the tweezers so that the dispersed phase was aligned perpendicular to the magnetic field. The influence of increasing the outer magnetic field on the droplet size and generation frequency, formed at a fixed flow rate, can be seen by viewing the micrograph sequences of FF droplet shown in Fig. 2a. The findings demonstrated that the diameter of the droplets decreased when B increased. However, the sizes of the droplets remained at an average diameter of 100 μm when B was increased further, but at B ca. 60 mT

Table 5　Advantages and disadvantages of substrates commonly used to fabricate devices for magnetic droplets generation

| Type of substrate	Advantages	Disadvantages	Ref
Glass	Optically transparent Hard Chemically and thermally resistant Biocompatible	Surface modification is required for oil-in-water droplet generation Expensive Fragile	[108]
PDMS	Optically transparent down to 300 nm Inexpensive and easy fabrication Good chemical stability Suitable for disposable chips Biocompatible	Surface modification is required for water-in-oil droplets generation Swell in the presence of some organic solvents It can absorb proteins and some hydrophobic molecules Stable up to 80 °C which can restrict some applications	[109, 110]
PMMA	Optically transparent Inexpensive Rigid Good mechanical stability Good chemical stability Suitable for disposable chips Biocompatible	Stable up to 125 °C which can restrict some applications	[111]
Fused silica	Commercially available with different diameters and coatings Ease of chemical modification	It can absorb hydrophilic molecules Fragile	[112]
Teflon and perfluorinated polymers	Commercially available Highly none sticky Moderate gas permeability Excellent chemical stability Thermally stable between −100-200 °C	Surface modification is required for water-in-oil droplets generation Difficult surface modification High electrical resistance	[113]

Fig. 1 a) Experimental setup for the formation of FF droplets at a microfluidic T-junction. The microfluidic device used to generate the FF droplet in silicone oil and the PDMS layer separating the glass and magnet with the flow direction are indicated. b) The effect of the continuous phase flow rate on Ca and the FF droplet size (the dispersed phase flow rate was maintained constant), the sizes are illustrated in photographs. Reprinted with permission from ref. [27]. Copyright (2010), IOP Science
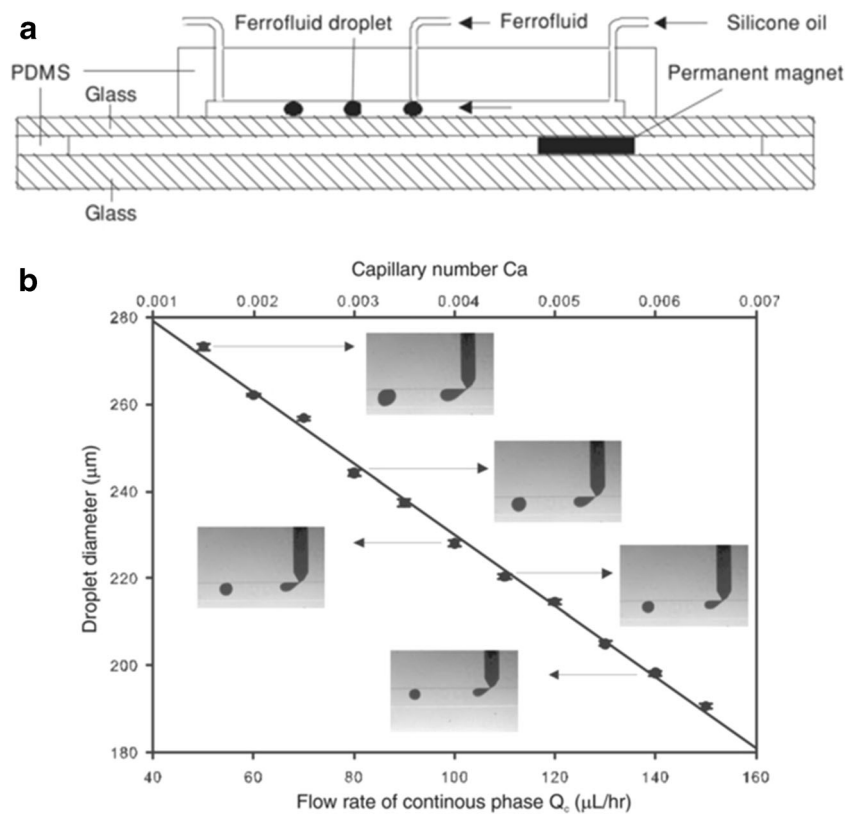
secondary droplets were generated and monodispersion of the droplets no longer existed. The influence of inner phase viscosity was also explored by comparing water and FF droplets under the same flow rate conditions. At a constant inner phase flow rate (Q_i), as the flow rate of the outer phase (Q_o) increased the droplet diameter decreased linearly. However, when Q_o/Q_i was higher than 7.5, the sizes of both water and FF droplets decreased slowly reflecting an independent behavior on the droplet size. The relationship between the maximum contraction positions of the FF tip and magnetic flux densities was also investigated (illustrated in Fig. 2b). A decrease in the distance between the maximum contraction position of the FF tip and the entrance of the throat (C_{max}) occurred initially as the magnetic flux density increases and then it reached a nearly constant value as the magnetic flux density was further increased. A smaller distance to the entrance throat resulted in a faster droplet formation frequency and, hence, a smaller droplet size. Additionally, these authors demonstrated that the magnetic droplets with different size distribution can be obtained utilizing different square wave signals. Using a low level area of the signal, larger droplets were generated, while smaller droplets were formed at a high level area of the signal. Thus, this method can be used to generate FF droplets with predetermined sizes and distributions. Ray et al. [53] investigated the effect of magnetic field on FF droplet size,

produced by using re-pumping mechanism which utilized an external magnetic field to generate FF droplets with tuned sizes. In this approach, a permanent magnet was placed at a certain distance from the droplet generation nozzle, defined as x = 0, and the distance between x = 0 and the droplet generation point was –x (0 - –5 mm) and a distance beyond the magnet is +x (0 – +5 mm). Droplets generated at the nozzle were called the initial FF droplet (IFD) whereas after merging at x = 0 they are called the final FF droplet (FFD). As the IFD approached a non-uniform magnetic field, several droplets merged and formed a slug because the hydrodynamic force created a larger FFD. The IFD size was governed by varying Q_d/Q_c, η, γ and diameter of the channel, and the FFD size was controlled by the applied magnetic field (H), Q_d, Q_c and the viscosity of the continuous phase. As H increased the size of FFD increased and reached a plateau at 10 mT, which was attributed to M_s and F_{mag}. Increasing Q_d and Q_c caused increase in the velocity and F_{drag} resulting in the formation of smaller FFDs. Furthermore, the FFD size was larger for silicone oil (85 mPa s) compared to heavy mineral oil (118 mPa s) due to the smaller F_{drag}. FF droplet generation and optimization using a pump-free approach was first described by Kakheshani and Di Carlo [54]. In this protocol, FF droplets were generated from a reservoir connected to multiple small channels solely using an external magnet
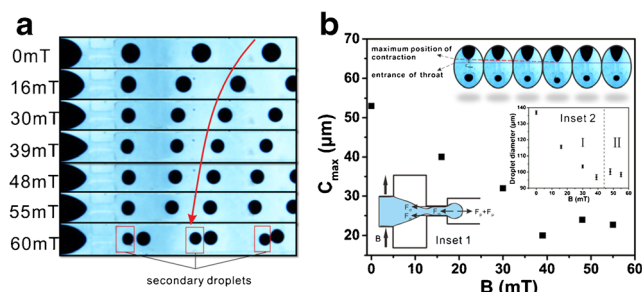
Fig. 2 (**a**) Micrographs of FF droplet under different magnetic flux densities. The red arrow demonstrates the effect of increasing the outer magnetic field on the droplet size and generation frequency (**b**) Maximum contraction position of the FF tip under the influence of different magnetic flux densities. The arrows indicate the distance between the maximum contraction position the entrance of the throat (C_{max}). Reprinted with permission from ref. [52]. Copyright (2015), Springer

placed underneath the device. The magnet dragged the FF stream towards an oil reservoir with dimensions larger than the channels in a pattern that mimics a 'step' in the terrace region (Fig. 3a–c). Droplets generated at the terrace region were a result of the presence of the magnetic force and the abrupt change in the interfacial tension at the FF/oil interface, which was caused by the increase in the channel dimensions. Due to the low flow rate and Re in this system, the inertial forces were negligible. The study focused on the size, generation frequency and mixing of droplets generated using only magnetic gradient. In comparison to effects arising from changes in the surface tension and magnetic field strength, the size of the droplets was found to be significantly influenced by the channel dimensions. The droplet size could be also controlled by modifying the length of the terrace. Specifically, when the terrace length increases from 60 to 90 μm the diameter of the generated droplets increased from 85 to 125 μm (Fig. 3d). While the droplet generation frequency was influenced by factors such as the interfacial tension, viscosity of the oil, volume fraction of the magnetic material, strength of the magnetic field and the number of channels connected to the FF reservoir. Furthermore, the results showed that interfacial forces were more important than viscous forces, as demonstrated by the observation that at Ca < <0.05 (equivalent to a flow rate 1 μL min^{-1}) droplet formation occured, whereas at Ca > 0.1 (equivalent to a flow rate 2 μL min^{-1}) the FF stream did not breakup and it stretched into the channel. Two different oils were used to investigate the effect of viscosity. The droplet generation frequency was found to be higher with Novec 7500 (η = 1.24 cP) than with FC-40 (η = 3.5 cP). Additionally, the device was modified to contain two and three inlets for introduction of the dispersed phase and studying mixing of reagents with the FF stream. For example, water and fluorescein were fed from separate inlets and

then mixed with ferumoxytol (a type of FF) to enable droplet generation. The intensity of fluorescein fluorescence intensity of the generated droplets was used to monitor the efficiency of mixing. The authors showed that the system had guaranteed mixing and can be employed to produce droplets of different sizes at different frequencies with controlled generation times (seconds to minutes). One limitation of this protocol was that magnetic properties must be incorporated in both dispersed phase streams in order to achieve droplet generation and complete mixing. Although significant studies have been conducted, methods for the continuous generation of magnetic droplets using magnetic forces still require further investigations that focus on other approaches including diamagentophoresis [55] and magnetic pumps [56].
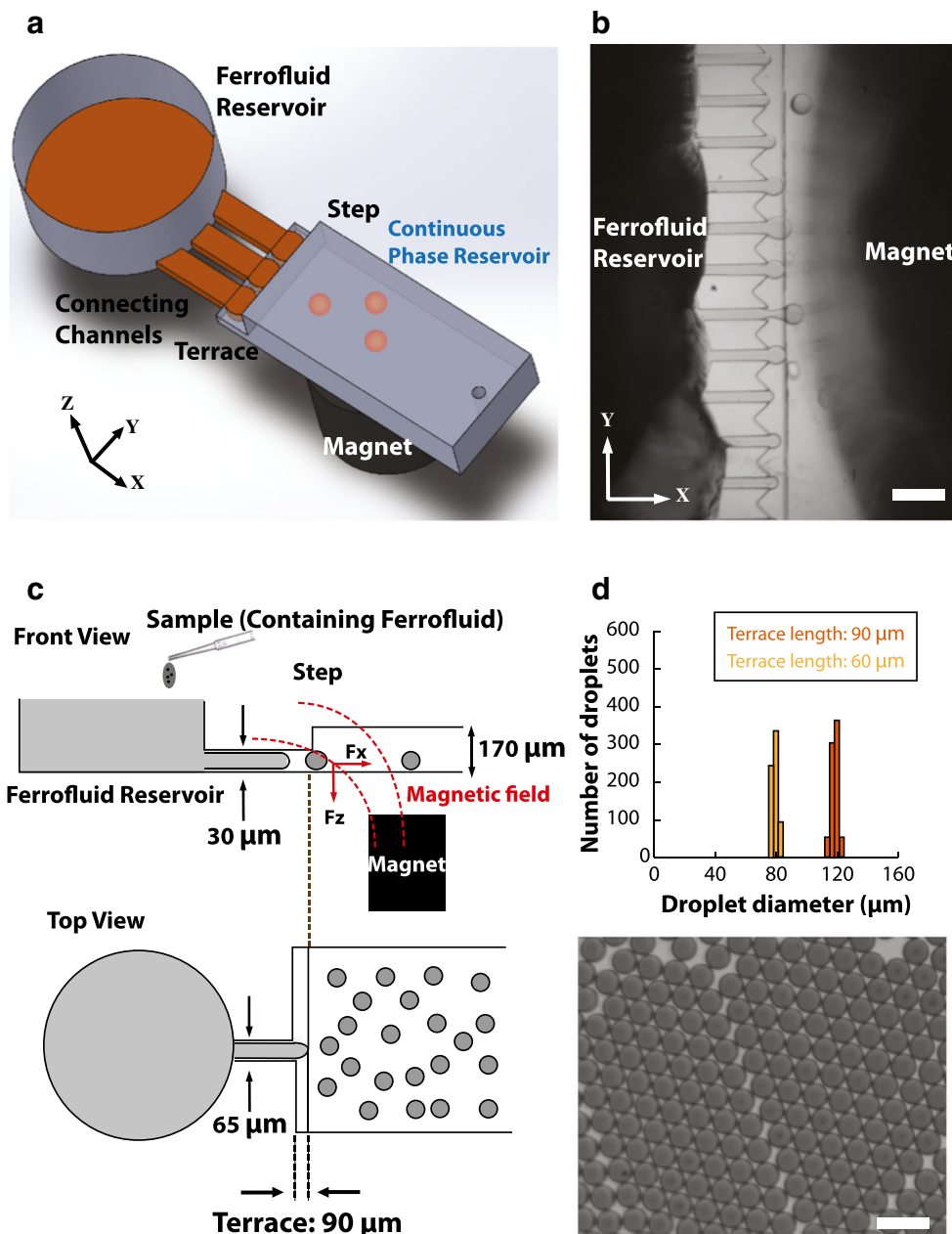
Manipulation of magnetic droplets

Methods for continuous generation and downstream manipulation of magnetic droplets are very appealing in that they enable rapid processing and screening of hundreds/thousands of droplets per minute with a high degree of control and precision. In this regard, approaches to controlled droplet generation, attraction, repulsion, sorting, trapping, splitting and coalescence in a continuous mode have been developed. In this regard, the on-chip free-flow magnetophoresis (FFM) principle has been applied for the first time to droplets [57]. Often, FFM is performed to sort particles/cells in continuous flow system with very high throughput [58], which makes the application of this technique ideal for processing hundreds/thousands of droplets in short time periods. This goal can be achieved by manipulating the magnetic field gradient and differences in magnetic susceptibilities between the magnetic objects and the carrier phases.

FFM, is a technique that utilizes magnetic forces to separate magnetic particles from each other or from nonmagnetic particles using a rectangular chamber, laminar flow and magnetic field [49]. The chamber has a number of inlets and outlets in the x-direction to maintain parallel flow with minimum mixing between the laminar streams, and a nonhomogenous magnetic field is applied in the y-direction (perpendicular to the streams). The magnetic force exerted on a magnetic particle introduced into the chamber causes it to experience a deflection of its path and to exit from one of the outlets close to the magnet. The particle will be dragged at a velocity (u_{defl}) equal to the sum (Eq. 5) of the hydrodynamic flow velocity u_{hyd} and the magnetically induced velocity u_{mag}, which is the ratio of F_{mag} (Eq. 4) and F_{drag} (Eq. 1) shown in Eq. 7 [25, 49]:

$$u_{defl} = u_{hyd} + u_{mag} \qquad (7)$$

Fig. 3 a) A 3D schematic of the magnetically driven droplet generation design displaying all the components, **b**) A photograph showing a FF droplet generated using a magnet by pulling from the reservoir, **c**) Front and top views of the platform showing the dimensions of the device, **d**) An image of the generated droplet, the droplet size was influenced by the size of the terrace as illustrated in the graph, scale bar 250 μm. Reprinted with permission from ref. [54]. Copyright (2016), the Royal Society of Chemistry (RSC)

Therefore, the magnetically induced velocity can be calculated from:

$$u_{mag} = \frac{N V \Delta\chi}{12 \pi r \eta \mu_0} \nabla B^2 \tag{8}$$

Zhang et al. [59–61] developed three systems for the continuous generation and manipulation of droplets in sealed microfluidic devices. The first system was designed for magnetic droplet attraction. In this system, a T-junction polydimethylsiloxane (PDMS) microfluidic device was used for generation, mixing and manipulation of magnetic droplets [59]. Superparamagnetic droplets containing Fe_3O_4 NPs suspended in water were synthesized by chemical co-

precipitation method. The microfluidic device consisted of a T-junction with two inlets to introduce the dispersed phase and a 400 μm chamber connected to three sub-microchannel outlets. In the absence of a magnetic field, the magnetic droplets followed a straight path (laminar flow direction) and exited via sub-microchannel 1. On the other hand, in the presence of a magnetic field generated by using a Nd-Fe-B magnet the droplets were deflected from the laminar flow direction at an angle (θ) and exit via sub-channels 2 or 3. The deflection angle can be calculated using the Eq. 9:

$$\tan\theta = \frac{2 \Delta\chi C r^2 B(\nabla B)}{9 \eta \rho \mu_0 v_x} \tag{9}$$

where C is the concentration of the magnetic NPs (in kg m^{-3}), r is the radius of the magnetic droplet (in m) and ρ is the density of the magnetic NPs (5.18×10^3 kg m^{-3}). The results of experimental studies showed that θ was proportional to the magnetic field gradient and MNPs concentration and was greatly affected by the position of the magnet. Superparamagnetic droplets and non-magnetic water droplets can be generated in an alternating manner using this platform. The two droplets were separated in the chamber by applying a magnetic field, which did not influence the flow path of the non-magnetic droplets so that they exited through sub-microchannel 1. In contrast, the magnetic droplets were deflected and exited via either sub-microchannels 2 and 3. This platform is suitable for rapid processing of superparamagnetic droplets and, thus, it finds potential utility in drug delivery/screening and immunoassays. Zhang et al. [61] also described the first magnetic repulsion systems to manipulate pL water droplets, which were modified versions of the platform previously used in droplet deflection [59]. While the original systems were utilized for splitting, dispensing, continuous-phase exchange, trapping, releasing and demulsification of water droplets, the continuous phase used in Zhang's system was magnetic [60, 61]. A similar system for deflection of the flow of magnetic droplets in a chamber and subsequent exiting via a desired outlet was also investigated by Al-Hetlani et al. [18]. In the deflection device, droplets of an aqueous FF were generated at a T-junction and deflected in a 2 mm wide and 6 mm long chamber using a small permanent magnet. The authors demonstrated that the field strength, position of the magnet, and magnetic loading influenced the degree of deflection. Another magnetic deflection platform was devised to sort single cells of *Thalassiosira eccentric* microalgae within magnetic droplets using magnetophoretic sorting method [62]. The system was designed to handle magnetic droplets of the same size (69.9 ± 1.1 μm) under the same conditions, containing the same number of MNPs at the same magnetic field strength. Upon introduction of cells into the droplet, the number of MNPs was reduced due to the displacement of the MNPs. Thus, the magnetic force acting on the droplet was decreased. In this device, the cells and MNPs were mixed off-chip and introduced from the same inlet to generate droplets at a T-junction. The droplets then entered a 'focusing region' to direct them to the side of the wall. After they exited in this area, the droplets were introduced into the 10 mm 'magnetophoretic separation region' causing them to deflect towards the opposite channel wall. The magnetic flux density in the system was enhanced by locating a nickel microstructure between the device and the magnet. This enabled separation of droplets containing both MNPs and single cells from pure magnetic droplets which were more greatly affected by the strong applied magnetic field. The authors showed that only 4.9% of the droplets contained single cells. The authors attributed this low level of encapsulation to the cylindrical

shape of the microalgae giving them a diameter of 39.9 ± 3.1 μm. Therefore, further improvement of this technique is required to develop a system for encapsulation of angulated and larger microalgae of *Thalassiosira eccentric*. An approach to deflect FF droplets across two immiscible streams having different interfacial tensions was investigated by Banerjee and co-workers [63]. The authors reported that the degree of deflection depended on an interplay between F_{mag}, non-inertial lift force (F_l) and interfacial tension force (F_i). Three flow regimes were designed based on varying the lift force ratio ($K_L = F_l/F_i$) and magnetic force ratio ($K_M = F_{mag}/F_i$), including no migration ($K_L << 0.44$ and $0 < K_M \le 0.14$), partial migration ($0.44 < K_L \le 0.46$ and $0.14 < K_M \le 0.16$) or 3) and complete migration from high to low interfacial tension ($K_L > 0.46$ and $K_M > 0.16$). The deflection of the droplets and migration length (L_{mig}^{*}) was found to depend on the location of the magnet (x_m^{*}) and the net force ($F_{R,net}$), which can be estimated using Eq. 10:

$$F_{R,net} = \left(\frac{F_m + F_l}{F_i} \right) \qquad (10)$$

At constant x_m^{*}, as $F_{R,net}$ increased L_{mig}^{*} decreased, whereas at constant $F_{R,net}$, increasing x_m^{*} resulted in an increasing L_{mig}^{*}. The effect of droplet size on droplet trajectory in the presence and absence of a magnetic field was also assessed. Interestingly, in both cases small droplets did not have a tendency to migrate to the second immiscible phase, while larger droplets moved across the boundary and entered the second phase. This phenomenon was attributed to the dependence of $F_{R,net}$ on the size of the droplet. This platform has the potential of being further expanded to studies of the migration of droplets between various streams of different interfacial tensions and viscosities related to drug deliver applications.

A method for continuous generation and downstream manipulation of magnetic droplets was also developed by Al-Hetlani et al. [18]. In this system, FF magnetic droplets were manipulated by using simple Nd-Fe-B magnets generated in a glass microfluidic device hydrophobized with a fluorosilane reagent. Droplets generated using a flow focusing design were split downstream at a T-junction to produce two daughter droplets, one magnetically enriched and the other magnetically depleted. In the absence of a magnetic field, the generated droplets approached the T-junction and split into two daughter droplets of equal size and content (Fig. 4a). When a magnetic field was placed near one of the T-junction arms, the MNPs within the mother droplet were attracted to the field and accumulate on one side of the droplet. Thus, splitting of these mother droplets at the junction creates pairs of magnetically enriched and depleted daughters (Fig 4b). The dynamics for splitting FF droplets at a T-junction microfluidic device under the influence of uniform (UM) and non-uniform magnetic fields was investigated by Wu et al. [64]. The system was
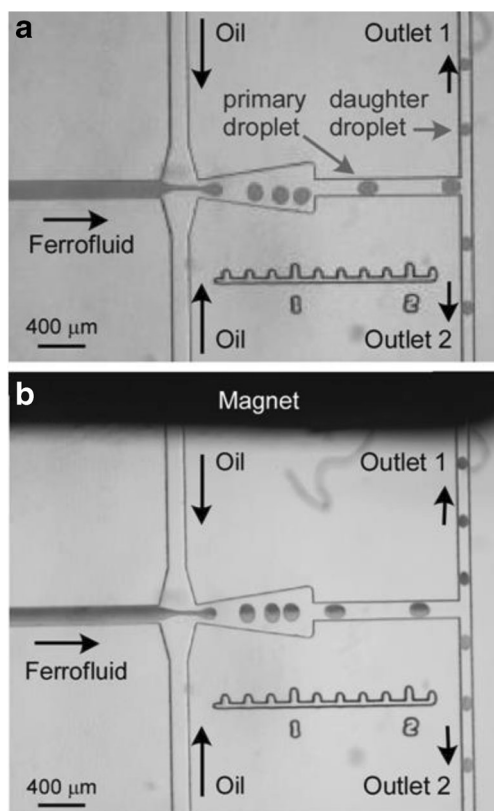
Fig. 4 Flow focusing manifold utilized in continuous generation and subsequent splitting of magnetic droplets using EMG 507 FF. **a**) Droplets generated and split in the absence of the magnet. **b**) Droplets generated and split in the presence of the magnet to produce magnetically enriched and magnetically depleted droplets. Reprinted with permission from ref. [18]. Copyright (2010), American Institute of Physics (AIP)

comprised of a flow focusing device with magnets placed at the two sides in order to form a UM and non-uniform (NM) magnetic field. Four droplet breakup regimes were explored including 1) permanent obstruction (BPO), 2) temporary obstruction (BTO), 3) without obstruction (BNO) and 4) non-breakup (NB). The difference between the breakup process of FF droplets using the BPO regime and under the influence of UM and NM was not clear. In these cases, the two dumbbell-like parts of the FF droplets break-up uniformly at the T-junction to form two daughter droplets. However, breakup of FF droplets using the BTO regime under a UM was associated with a much larger channel compared to that occurring under a NM. Following stretching caused by the magnetic field, the droplets broke into two symmetric daughter droplets. Additionally, the breakup process using the BNO regime displayed similar behavior under both UM and NM conditions. In this case, the droplets stretched at the T-junction, moved to the wall opposite to the feed channel and upon impact broke up into two daughter droplets. In the case of the NB condition, droplets emerged from the T-junction and enter either of the bifurcations based on feedback formed by the preceding droplet. Breakup at the T-junction was mainly

affected by the droplet size (L) or the dimensionless droplet length ($\varepsilon = L/\pi W_c$, W_c is the width of the channel), and Ca. Therefore, the behavior of the droplet as a function of Ca was probed using four magnetic flux densities. The results showed that as the magnetic flux density increased, the BTO region gradually enlarged towards BPO. This phenomenon was attributed to elongation of FF droplets due to the effect of the magnetic field [40, 65]. The FF droplet stretched in the direction of the uniform magnetic field, which is parallel to the branches of the T-junction. Hence, the two dumbbell-like parts separated from the wall enabling a higher flow of the continuous phase into the bifurcations. B_0 was also introduced to determine the stability of the shape of the droplets. Moreover, the authors substantiated that the uniform magnetic field cannot only influence the type of breakup but also the breakup process. The results of this effort demonstrated that the breakup of FF droplets in the presence of a non-uniform magnetic field generated two daughters of different sizes into either side of the bifurcation. Moreover, the volume ratio of the droplets flowing in the right and left branches (V_R/V_L) was influenced by the total flow rate $Q_t = Q_c + Q_d$. Therefore, this study has provided an insight into the behavior and mechanism for breakup of FF droplets and has demonstrated how to control the size of the droplet using an additional and controllable external force. Controllable breakup of FF droplets at a simple Y-junction in a microfluidic device was investigated by Li et al. [66] using a magnetofluid technique. At the Y-junction divergence in the system, the mother droplet split into two identical daughter droplets, which was in agreement with the previously reported observations [67]. However, placing an external magnet on the side of the upper arm of the microchannel caused asymmetric breakup of the mother droplet to occur, in which the forefront was pulled up into the upper arm due to strong non-uniform magnetic attraction. Subsequently, the size of the daughter droplet in the upper arm increased gradually as the injection liquid continued to flow (Fig. 5a). A probe of the influence of the flow rate ratio (Q_d/Q_c) showed that respective symmetric and asymmetric size distributions were obtained in the presence and absence of an external magnetic field (Fig. 5b). Additionally, the size of mother droplet decreased as Q_d/Q_c decreased while the asymmetric size distribution increased. Furthermore, the volume ratio of the daughter droplets (V_u/V_l) as a function of Q_d/Q_c at various magnetic flux densities was explored. The findings indicated that the influence of Q_d/Q_c was insignificant in the absence of the magnetic field and V_u/V_l remained 1. However, in the presence of an external magnetic field, V_u/V_l decreased as Q_d/Q_c increased and remained almost constant when $Q_d/Q_c > 1$. The latter observation was ascribed to the large length of the mother droplet, which retarded the rupture of the droplets thereby slowing their growth rate. Additionally, it was found that when Q_c increased to 20 mL h^{-1}, the droplets did not breakup and are instead pulled towards the external
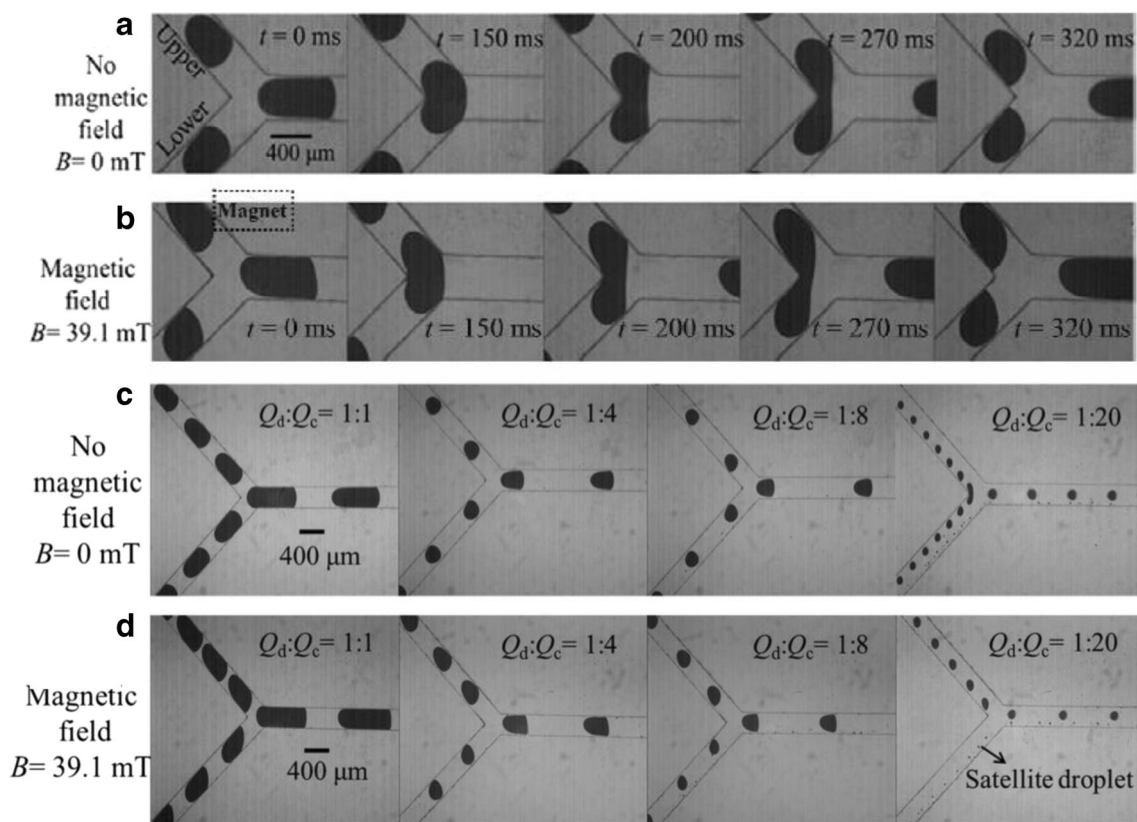
Fig. 5 **a–b**) The breakup of FF mother droplet at a constant flow rate ($Q_d = 1$ mL h^{-1} and $Q_c = 2$ mL h^{-1}) at the Y-junction **a**) without and **b**) with the external magnet. C-D) The effect of the flow rate ratio on the FF droplet distribution at $Q_d = 1$ mL h^{-1} a symmetric distribution was obtained in the absence of magnetic field and D) An asymmetric distribution was generated in the presence of a magnetic field. Reprinted with permission from ref. [66]. Copyright (2016), the Royal Society of Chemistry

magnet while undesired satellite droplets moved into the lower arm. Finally, theoretical simulation based on B_o was carried out to predict the size of the daughter droplets. The numerical values arising from this treatment showed that FF droplets with desired sizes can be generated by optimizing the fluid flow rate and the magnetic flux density [66]. Further details of asymmetric FF droplet splitting at a T-junction have been elucidated using theoretical numerical investigations [68]. Analysis and optimization of factors that influence the extraction of magnetic particles at a splitting fork were carried out by Brouzes et al. [44]. The principle of the system was to marginalize the magnetic microparticles within moving droplets by using an external magnetic field prior to their split at a fork (rather than T- or Y-junction). The authors determined the optimal position of the splitting fork relative to the magnet. For this purpose, an imaginary "midline" was drawn across the middle of the droplet, which split the droplet into an upper or "waste" and lower or "enriched" parts. The results showed that the enclosed magnetic particles tend to aggregate at the upper and lower parts of the droplet as it moved past the magnet resulting in concentrating the majority of the particles in the lower part of the droplet. Next, a determination of the fraction of particles in the midsection of the droplet as a function of the droplet velocity and magnetic force showed that the

particle fraction and magnetic field strength was not linearly related, which was difficult to interpret due to the formation of particle chains within the droplets. A 1:1 symmetric split fork with "upper" and "lower" branches was used to study splitting and enriching efficiencies as a function of droplet velocity and magnetic force. Using a splitting fork width that was half that of the main channel led to production of identical sizes of the droplets. At 20 and 60 pN, the approximate number of particles in the "waste" droplet was small at low velocities (< 2%), but increases (>6%) as the velocity increased. The efficiency of particle separation at the 1:1 symmetric splitting fork depended on the droplet velocity and generation frequency. To minimize the amount of particles deposited in the "waste", the droplet size was reduced by adjusting the splitting ratio and profile. The splitting ratio was controlled by using an asymmetric splitting fork whereas the profile was controlled by manipulating Ca (lower values being more favorable). At low Ca and constant velocity, the fork design highly influenced the enrichment of the particles with optimal enrichment occurring when a 1:3"upper" and "lower" branch ratio, 50 μm hydraulic resistance and along box, was utilized. Moreover, the enrichment increased as Ca increased and then plateaued at 0.27, which corresponded to the value at which interfacial tension can be neglected. The authors proposed that

their system can be employed for the detection of a threshold of highly expressed genes and supported it by comparing the theoretical predictions with earlier experimental findings those found earlier [45]. However, no experimental data was provided to substantiate the proposal.

Generation of magnetic double emulsion was first explored by Sander et al. [69]. Nanoliter magnetic droplets have been generated using a commercially available FF in the form of a single or double emulsion in a microfluidic device. The magnetic cargo containing emulsions were transported, collected and coalesced by controlling the external magnetic field. The emulsions used in this study were oil-in-water (O/W) droplets and double emulsions of water-in-oil-in-water droplets (W/O/W) and the cargo was contained in the inner oil, water droplet or the intermediate oil phase of the double emulsion generated within the device. The FF was mixed with the inner phase of the single emulsion (MO/W), and the intermediate (W/MO/W) or inner phase (MW/O/W) of the double emulsion by introducing magnetic particles into different fluids in the emulsification step. MO/W droplets were too stable to enable rupture of the droplets, which was ascribed to the presence of a surfactant in the commercial FF. However, the use of high concentrations of $CaCl_2$ in combination with a strong magnetic field enabled more proficient droplet coalescence. The coalescence force was estimated to be 50 nN for the MO/W in the presence of $CaCl_2$ and the magnetic field required to achieve coalescence was ca. 75 Oe. On the other hand, destabilization was not required for the MW/O/W and W/MO/W and the aqueous magnetic droplets in these cases broke through the oil layer and entered the continuous phase. Furthermore, a fluorescent reagent was incorporated into the double emulsion system in a manner that leads to creation of a magnetic core and a fluorescent intermediate layer to avoid mixing. At high magnetic fields, the thin films separated into individual droplets that led to coalescence into one large droplet. Another double emulsion platform devised by Misuk et al. [70] involved the use of an organic solvent (toluene or cyclohexane) and paramagnetic ionic liquid (MIL). In a surfactant-free approach, the magnetic inner sphere of the emulsion droplets, composed of 1-butyl-3-methylimidazolium cation and a paramagnetic anion of iron, manganese, nickel or dysprosium, were synthesized in an off-chip manner using a previously reported procedure [71–73]. Merging the MIL with the organic phase at the first T-junction produced MIL droplets, which then travelled through the inner capillary where they merged with a perfluorinated solvent at the second T-junction to generate the double emulsion of organic phase/MIL/FC-40. A magnetic field simulation was used to gain information about the effect of the strength of the magnetic field on the flow behavior of the double emulsion droplets. The use of two external Nd-Fe-B magnets enabled controllable manipulation of individual emulsion droplets including capture, release, pair-merging, coalescence, separation and reunification.

Moreover, the efficiency of pair-merging was visualized by utilizing two commercially available ink containing colored streams of the double-emulsion droplets within a Y-junction. Unlike in microfluidic devices, in the capillary-microreactor using organic solvents pre-treatment of the device surface was not required and low and high flow rates of the solvents were achieved [70]. A coaxial capillary microfluidic system comprised of MIL of [bmin]$FeCl_4$ was used to generate magnetic droplets [29]. The coaxial device consisted of a capillary, used for injection of the dispersed phase, coaxially aligned with a second capillary (inner diameter = 0.70 mm) with tapered orifice of approximately 70 μm inserted into a second larger capillary (inner diameter = 1.05 mm) to pump the continuous phase. The effect of magnetic field strength and flow rates on the flow pattern and droplet size was assessed and a mathematical model for predicting the droplet size was developed. Additionally, the ability to control coalescence of the generated MIL droplets by tuning the applied magnetic field was demonstrated. In the absence of a magnetic field, the MIL droplets behaved like normal Newtonian fluids and dripping (at low Q_c and Q_d) or jetting regimes (at high Q_c and Q_d) was observed depending on Q_c and Q_d. Dripping was used in experiments employing inhomogeneous magnetic fields along the coaxial capillaries. The effect of the magnetic field strength on droplet generation was influenced by the distance between the frontier of the magnet and the capillary orifice (x). Increasing magnetic field strengths caused acceleration in droplet breakup and generation of small fast-moving droplets. The effect of Q_c on the droplet was investigated by fixing Q_d and x, and varying Q_c between 100 to 300 μL min^{-1}. Compared to those created in the absence of a magnetic field, droplets created using Q_c = 100 and 300 μL min^{-1} had diameters reduced by 27.5% and 8.3%, respectively. This finding showed that the effect of magnetic field strength has a more pronounced effect on droplet size than viscous forces. In the presence of the magnetic field, smaller droplets were obtained due to the accelerated rate of droplet formation. A modification of this device was developed that enabled injection of two dispersed phases (magnetic and non-magnetic) for in situ generation and coalescence of droplets. In the process, the magnetic droplets were trapped by use of the magnetic field and subsequently merged with the flowing non-magnetic droplets. Due to viscous forces, the mixed droplets were released from the influence of the magnet and moved in the direction of the hydrodynamic flow. Despite the fact that double (or more) emulsions exhibit interesting structures and can be formed in droplets with high precision, thus far they have not been employed in any applications. Furthermore, double emulsions can be converted to solid particles (as will be discussed in section 3.2) and can be used as potential drug carriers.

Lin et al. [74] developed the concept of hybrid magnetic-optical joint barcoding and decoding droplets in a magnetofluidic device. The device was comprised of an

encoding area, storage pool and magnetic decoding area containing integrated giant magnetoresistive (GMR) sensors. The optical component employed in the system was a fluorescently labeled penicillin (P) derivative serving as a model drug and MNPs were used as the magnetic component. In addition, P, MNPs and water were encapsulated within droplets in the encoding area using mineral oil. After their formation, the droplets were first directed into a reservoir (pool) to enable the optical observation, and were moved into the decoding area with the aid of an additional oil stream arising from a side channel. This protocol was used to avoid optical interferences when collecting the GMR signal. Final decoding of the magnetic and optical barcoded droplets was achieved using respective fluorescence (a.u.) and magnetic voltage (μV) signals for the quantification of the MNPs and P the signals were measured simultaneously as the droplets passed through the decoding area. The intensities of the recorded signals varied with the amount of the MNPs and P in the droplet, which were controlled by Q_c and Q_d. The sensitivity of the system was determined using standard deviation values (σ) which were found to be ca. 1.5 μV and ca. 1.6 a.u. for the magnetic voltage and fluorescence intensity, respectively. These values indicated that ca. 96% of the droplets were produced within a confidence interval of 2σ. Although in this effort the detection frequency of the formed droplets was 10 droplets per second it can be increased by increasing the Q_c and Q_d. For instance, increasing Q_c from 30 to 900 nL s^{-1} and MNPs stream from 10 to 100 nL s^{-1} reduced the droplets size from 150 to 80 μm, which caused the detection frequency to increase to ca. 240 droplets per second. Moreover, the amplitude of the GMR signal was decreased by a decrease in the droplet size so that a minimum droplet size of 60 μm can be detected by the GMR. This coded magnetofluidic device has the capability of dual fluorescence and magnetic detection of multiple components present in the same droplet, and, as a result, it can be further utilized to perform assays like those quantifying the amount of fluorescently labeled cells compared to the amount of MNPs located in a single droplet.

Microfluidic devices that utilize a combination of conventional PDMS and replica molding techniques were developed by Teste et al. [75] for selective treatment of magnetic droplets. In the fabrication process, a PDMS pre-polymer was mixed with ferromagnetic iron microparticles (6–8 μm) and poured into an aluminum mold (Fig. 6i a). After degassing, a soft silicon blade was used to remove excess magnetic PDMS followed by spreading the PDMS pre-polymer on top of the mold. Following incubation of the system at 70 °C for 15 h (Fig. 6i b-c), the resulting structures were peeled off and planarized by adding fresh PDMS using a salinized glass slide with a scotch tape spacer (Fig. 6i d-e). The system was then kept at 70 °C for 2 h before the bottom of the structure was integrated in the magnetic rail and bonded to the microchamber. Finally, the inlet and outlet of the device were

connected via Teflon tubing (Fig. 6i f-i) and the thickness of the final PDMS layer on the top of the rail was 50 μm. The microsystem was inserted into a home-made electromagnetic coil controlled by a tunable power supply to generate a homogenous magnetic field at the center of the coil. In the absence of the external magnetic field, the trajectory of the magnetic droplets in this devise was linear, indicating that the droplets were dragged by the oil flow only. However, when the external magnetic field was on, the rails induced an attractive force that stimulated formation of magnetic clusters, which caused the motion of the droplets to deviate from their linear path. Furthermore, droplet sorting, parking and merging were performed using a microdevice that combined the magnetic rail network and an array of physical traps (Fig. 6ii). Switching on the external magnetic field allowed the droplet to pass over the first rail (r1) and be trapped. Similarly, the following droplets can be sorted and trapped in rails r2-r4 and by reversing the flow, the droplets can be made to flow back to the inlet streamline. Additionally, merging of the droplets can be performed using the same concept. For example, after trapping the first droplet, a train of additional droplets can then be introduced. Once the droplets are in contact, increasing the flow rate to >15 μL s^{-1} caused the droplets to merge. A study using an enzymatic reaction was performed to demonstrate the potential use of the system for monitoring of processes occurring within a single droplet. Although the system enables controlled sorting, parking and merging of droplets, as well as performing enzymatic reactions, fabrication of the device was complicated and time consuming.

Varma et al. [76] was the first to conduct an experimental and modeling investigation of uniform magnetic field induced merging of FF droplets. The use of uniform magnetic fields enabled contact-free, wireless programmable control of magnetic droplets. In the device, FF droplets were generated at a T-junction configuration utilizing a squeezing regime (i.e. Ca < 10^{-2}) and alternating droplets were generated at the T-junction by having two inlets for the dispersed phase facing each other. The uniform magnetic field was generated using a water cooled DEXING electromagnet system with an air gap of 4 cm between the magnet poles, and the microfluidic device was mounted in the middle of the poles. Independent dye and FF droplets were generated at a constant flow rate ratio in the absence and presence of the uniform magnetic field. Due to the attraction force of the magnetic field, a decrease in the generation time took place. On the other hand, an increase in the droplet size occurred as H increased to 500 mT. However, a further increase in H to 1000 mT caused the field to become non-uniform which resulted in elongation and an increase in the surface tension of the FF droplets. An assessment of the FF droplets merging in the presence of a uniform magnetic field was carried out by varying H and merging length (Lm), which is the distance from the T-junction to the center of the droplet at the droplet merging point. In the presence of the field, a

i`

ii
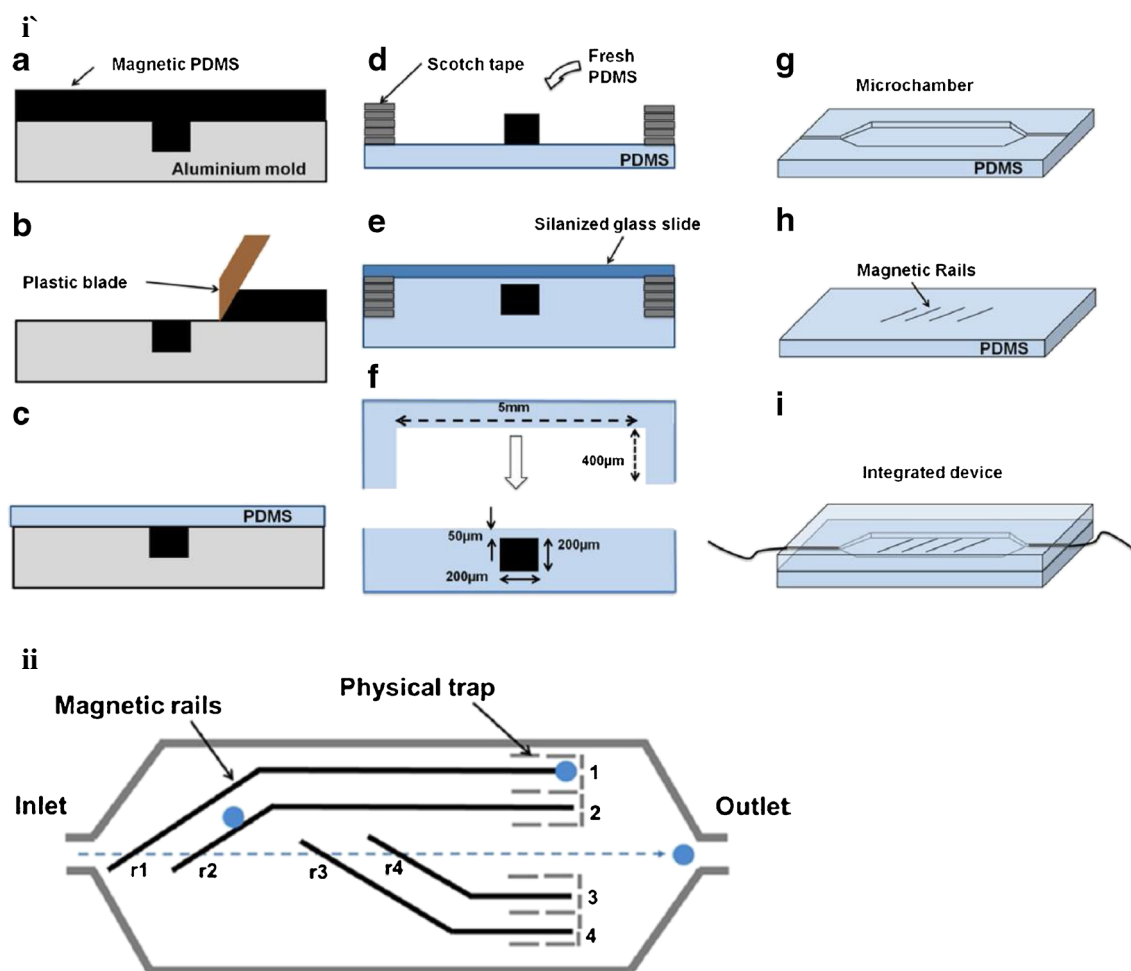
Fig. 6 (i) A detailed schematic representation of the microfluidic platform where the bottom part was integrated with the magnetic rail structures. (ii) Schematic representation of the microdevice used to sort, park and merge the magnetic droplets showing integrating a magnetic rails network and physical traps array . Reprinted with permission from ref. [75]. Copyright (2015), Springer

competition existed between fluidic pressure, which depends on Q_p and Q_c, surface tension and magnetic force. Merging will take place only when the magnetic force exceeds the sum of the two other forces. Droplet merging was studied at a constant H of 500 mT and different droplet velocities, particularly at flow rate ratios of 2 and 5. Assuming that two consecutive droplets with velocities V_a and V_b merge to form a droplet with velocity of V_{ab}, three scenarios can exist for successful merging of two droplets with respect to variations in V_a and V_b, including i) both droplets moving in the same flow direction and $V_a < V_b$, ii) both droplets moving in the opposite flow direction and $-V_a > -V_b$, and iii) both droplets flow towards each other. At $t = 0$ the transition merging point, $V_b - V_a$, reached a maximum value and droplets are then merged. The results of time variation simulations of velocity were found to be in agreement with the experimental results. Application of the magnetically induced merging technique was demonstrated by generating FF and blue dye droplets in oil. In the absence of the magnetic field, no droplet merging tooke place while at H = 1000 mT the droplets merge to form

green FF droplets. The authors suggest that the system can be used for biosensing, bioassays and determining reaction kinetics.

Fabrication of magnetic materials in droplets

The synthesis of magnetic materials within droplets has received great attention. The fabricated magnetic materials have been found to have small and narrow size distributions, in addition to interesting morphologies. Among the materials that have been prepared in this manner are MNPs [77], magnetic microstructures [78], magnetic Janus particles [79] and magnetic hydrogels [28].

Synthesis and modification of MNPs

Due to the existence of highly controlled mixing and reaction conditions within droplets, it was believed that it would be possible to generate particles with small sizes and

monodispersities in this environment, Table 6. This proposal was initially explored by Frenz et al. in 2008 [77] in the context of continuous synthesis of iron oxide NPs using controlled electrocoalescence of two droplets. Mixing of the first droplet containing a mixture of Fe^{2+} and Fe^{3+} precursors with the second containing ammonium hydroxide produced iron oxide NPs. The electrocoalescence device employed for this purpose consisted of two hydrodynamically coupled nozzles and a central oil channel. When the first primary droplet was formed, the aqueous stream blocked the oil channel causing an increase in the flow of oil through the second nozzle to produce a secondary droplet. Once the secondary droplet was generated, the oil flow moved back to the first nozzle enabling the formation of the second primary droplet. Within the PDMS device, electrodes were programmed to pair the droplets and promote electrocoalescence, which was effectively accomplished when the droplets were generated at flow rate ratios of 1:1 and up to 1:5. A preliminary evaluation of the efficiency of electrocoalescence and mixing of the two alternating produced droplets was conducted by mixing using two fluorescent dyes. The results showed that droplet pairing occured to the extent of 99.99%. The results of off-chip characterization of the MNPs prepared using this system by TEM showed that they had an average particle size of 4 ± 1 nm, in addition to displaying hysteresis in the magnetization curve, which confirmed their superparamagnetic nature. Another droplet-based microfluidic system for synthesizing biogenic FeMn MNPs was described by Jung et al. [80]. In this system, a flow-focusing configuration was used to generate nL droplets containing E. coli cells and a mixture of $FeSO_4 \cdot 7H_2O$ and $MnCl_2 \cdot 4H_2O$. The droplet contents were thoroughly mixed, using a device having a serpentine channel design, and then incubated on-chip in a chamber for 5 min and off-chip for 18 h at 37 °C. Laser-induced confocal microscope analysis showed that while the size of the droplets remained constant and that the color of the cells changed to brown as a result of formation of biogenic NPs were in their interiors. After droplet breakage, the E. coli containing FeMn NPs were collected in eppendorf tube. The cells were then isolated by using a magnet, washed by using ultracentrifugation and calcinated to eliminate any

proteins that might have bound to the NPs. The biogenic NPs were characterized off-chip using TEM and a vibrating sample magnetometer (VSM). The size of the on-chip prepared NPs was determined to be 5.17 ± 0.24 nm, compared to the smaller yet slightly polydispersed off-chip NPs that have a size of 3.04 ± 0.68 nm. The magnetization profile of the NPs obtained in the range of -5.0 to $+5.0$ kOe did not display saturation or loss of their magnetism, confirming the paramagnetic nature of the particles. Interestingly, a capillary based microfluidic device that enables droplet mixing, flocculation, magnetic decantation, colloidal re-dispersion, washing, surface functionalization, heating and colloidal assembly was developed for the synthesis of MNPs by Ferraro et al. [81]. Using this device, fluorescence labeled and amine functionalized silica NPs (SiO_2 NPs, 200 nm) were coupled with citrate functionalized FF (γ-Fe_2O_3, 9 nm) under pH controlled conditions using a trapping mechanism. Initially, a droplet containing γ-Fe_2O_3 NPs was trapped using magnetic tweezers and then merged with another droplet containing trisodium citrate. This caused destabilization and precipitation of the NPs within the droplet. A homemade heater was used to enhance diffusion and grafting of the citrate molecules on the surface of the NPs. Then, a droplet of functionalized γ-Fe_2O_3 NPs was formed, trapped in a capillary using the magnetic tweezers, and subjected to washing steps with droplets containing a mixture of acetone/water and two droplets of water. Then, the NPs cluster was added to 3-(N-morpholino)propanesulfonic acid (MOPS) buffer droplet. Finally, the citrate functionalized MNPs suspended in MOPS were trapped and merged with a droplet, containing the fluorescent material Rhodamine B isothiocyanate-SiO_2 (RITC-SiO_2 NPs), to form a droplet containing magnetic nanoassembly of RITC-SiO_2@ γ-Fe_2O_3. Inspection of fluorescence images demonstrated that the nanoassemblies present in the droplet were randomly oriented in the absence of a magnetic field while in the presence of the magnetic field the NPs became aligned along with the direction of the field. Moreover, TEM analysis proved that γ-Fe_2O_3 NPs were attached to the surfaces of the RITC-SiO_2 NPs.

**Table 6** Summary of MNPs and their advantages and disadvantages generated in magnetic droplets

MNPs	Advantages	Disadvantages	Ref
Iron oxide (type not specified)	Commercially available Different surface functionalities Superparamagnetic	Type not specified in the publication	[77]
γ-Fe_2O_3	Commercially available Different surface functionalities Superparamagnetic Biocompatible	A product of the oxidation of Fe_3O_4 Lower M_s compared to Fe_3O_4	[81]
FeMn	Paramagnetic	Not commercially available	[80]

Synthesis of magnetic microstructures

In 2011, magnetochromatic microcapsules were prepared using droplet microfluidics by Zhu et al. [82] for array display applications (Fig. 7a–c). The microcapsules, composed of an aqueous suspension of magnetic nanospheres covered with a transparent layer of ethoxylated trimethylolopropane triacrylate (ETPTA) resin. ETPTA was chosen for this purpose due to its fast solidification time when exposed to UV radiation, transparency and density which closely matches that of water. In an off-chip procedure, oleic acid modified Fe_3O_4 nanocrystals were mixed with styrene, methacrylic acid, hexadecane, water and sodium dodecyl sulfate (SDS) to form magnetic nanospheres, which were then suspended in water. The magnetochromaic microcapsules were produced using a droplet platform composed of a double T-junction channel with three syringe pumps to deliver the three reagent streams. The inner aqueous phase was composed of magnetic nanospheres, the middle phase contained ETPTA and a photoinitiator, and the outer phase was comprised of water mixed with surfactant (4% polyvinyl alcohol, PVA). This system generated monodispersed magnetic core-ETPTA shell double emulsion droplets, which were subsequently collected off-chip in a glass dish and exposed to UV light for 15 min to promote solidification. The magnetochromatic microcapsules were then formed with an average size of ca. 138 nm (Fig. 7b)

by placing the microcapsules into a single layer, close-packed hexahedral array and adding a boiling aqueous solution of agarose to fill the gaps between the microcapsules. Upon cooling to room temperature, microcapsules having different colors and patterns were formed. Characterization of the formed microcapsules was conducted using optical techniques including digital microscopy and scanning electron microscopy (SEM) to assess their magnetochromatic behavior, shape and morphology (Fig. 7a). The change in color of the array was completely reversible process, the coloration of the array changed under different magnetic stimulations and returned to its original state when the field was removed, as shown in Fig. 7c. One dimensional chains of connected soft droplets were synthesized for the first time within a single microfluidic device by Jiang et al. [83]. The simple platform was comprised of a T-junction to form aqueous chitosan droplets in oil and surfactant, and a side channel to deliver a mixture of an incubation phase of glutaraldehyde (GA), oil and surfactant. The role of the surfactant was to stabilize the droplets and that of GA was to covalently crosslink the chitosan droplets as they flowed through the serpentine channel to form a chain, which was eventually collected in a reservoir. The optimum conditions for preparation of 150 μm droplets involved a generation rate of one droplet per second, although higher frequency and larger sizes can be obtained. This strategy was employed to fabricate magnetic, magnetically fluorescent and fluorescent/
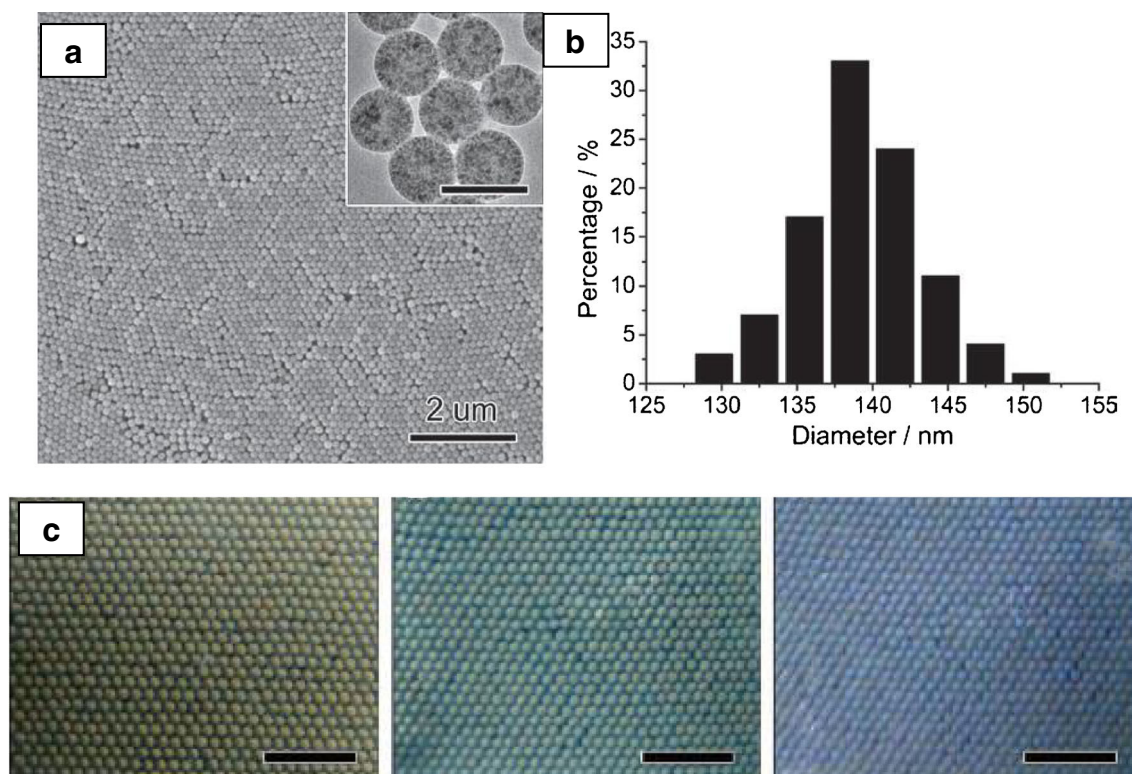
Fig. 7 **a**) SEM image of the magnetic nanospheres encapsulated in microcapsules, the inset is a TEM image of the nanospheres (scale bar 200 nm), **b**) Size distribution of the synthesized magnetic nanospheres and **c**) Digital photograph of the coloration of the array as the strength of the magnetic stimulation changes. All scale bars are 2 mm. Reprinted with permission from ref. [82]. Copyright (2011), Wiley

non-fluorescent alternating chains. Magnetic chains were obtained by adding γ-Fe$_2$O$_3$ NPs (average surface area ca. 42 m^2 g^{-1}) to the chitosan solution and incubating the chains within the microchannel for 24 h. The stiffness of the chains was found to depend on the time for incubation of the droplets in GA, with longer incubation times (24 h) leading to rigid rodlike chains and a short 5 min incubation time resulting in production of flexible chains. The presence of magnetic functionality enabled the chains to be controlled using an external magnet (Fig. 8).

Bokharaei et al. generated non-magnetic and magnetic polymeric droplets using a flow focusing device [84]. The dispersed phase used in this system was 10% poly(L-lactic acid) (PLL) in chloroform and the continuous phase was 2% PVA in water. The PLL droplets were collected off-chip in a 2% solution of PVA followed by solvent removal using an 8 h air flow. Addition of MNPs to the dispersed phase required a re-optimization of the flow rates due to irregularities in Q$_d$, mainly as a result of the change in phase rheological properties. Different amounts of the MNPs were incorporated to produce droplets with different sizes and magnetic properties. The particle sizes were found to be in the range of 24.06–31.66 μm and their saturation magnetization (M$_s$) occurred between 11.1–13.1 emu g^{-1}. A determination of their heat generation capability, also known as specific absorption rates (SAR), at a constant frequency displayed a small decrease as the number of the MNPs decreased. Inspection of SEM images showed that the non-magnetic microparticles were spherical and had smooth surfaces. On the other hand, the magnetic microparticles had porous and uneven surfaces. These phenomena can be attributed to the rate and mechanism of solvent removal or drug release during the solidification process. Furthermore, the authors developed a 3D computational multiphase droplet generation model, which produced results that

correlated well with the experimental data. The microparticles produced in this manner had a high potential for magnetic hyperthermia applications and drug delivery. In another effort, a droplet microfluidic platform for the synthesis of magnetic microspheres with controlled macroporosity was developed by Paquet et al. in 2012 [78]. By combining MNPs with a polymer, it was possible to form functional magnetic microparticles with controlled sizes, porosities and narrow size distributions without the need for chemical transformations such as polymerization. The formed droplets, containing a mixture of iron oxide NPs, poly(styrene/maleic anhydride) and an organic solvent, were collected off-chip in a solution of SDS, where the solvent diffused out of the droplet. The results showed that the diameter of the microparticles was influenced by Q$_c$/Q$_d$ and had a CV of 2–3%. Two critical factors affecting the morphology of the generated microspheres include the concentration of SDS in the collection solution and the nature of the solvent. Inspection of SEM images of microspheres created using SDS concentrations between 0 and 250 mM revealed the existence of large differences in the morphology depending on the SDS concentration (Fig. 9a–f). For example, with SDS concentration $\leq$ 10 mM the microparticles were densely compact composites of the NPs and polymer, whereas at SDS concentrations >100 mM the microspheres had denser channel-like structures. Additionally, the sizes and stabilities of the collected droplets were found to depend on SDS concentration (Fig. 9g and h). The effect of solvent was investigated using chloroform, toluene, hexane and a mixture of tetrahydrofuran (THF) and toluene. The droplets were observed to form particles after a few minutes when chloroform was used, whereas longer times were required for particle formation when other solvents were utilized. However, a denser pore structure was formed when hexane or a THF/toluene mixture was used. The results of nitrogen isotherm

Fig. 8 Successive photographs of semiflexible magnetic chains generated in droplet microfluidics in continuous flow moving under the influence of the magnetic field. Reprinted with permission from ref. [83]. Copyright (2011), Wiley
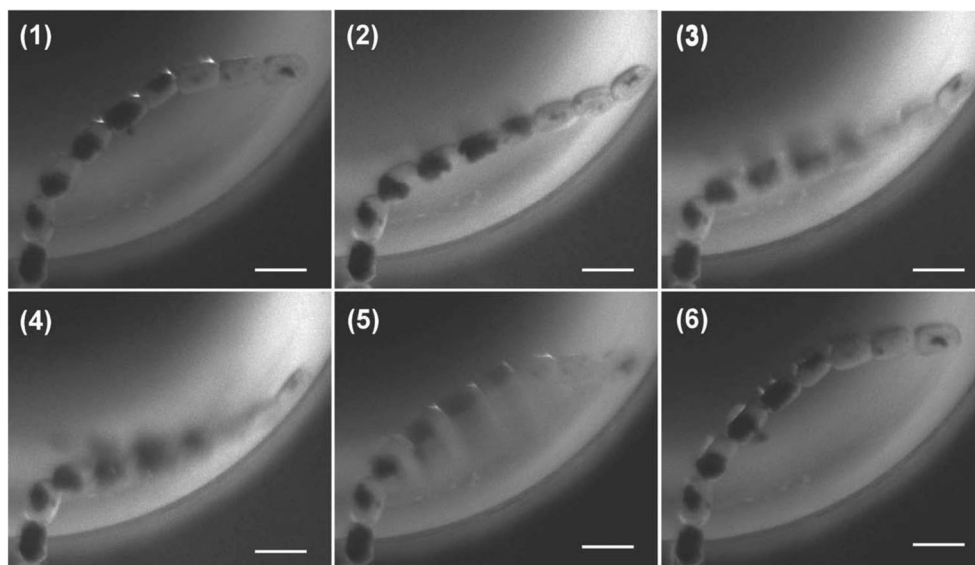
measurements and Brunauer-Emmett-Teller (BET) calculations on the magnetic microparticles produced using 25 mM SDS showed that the surface contained macropores (d > 50 nm) and a total surface area of 5.2 m^2 g^{-1}. This method can be used to prepare novel and versatile materials, such as porous magnetic microspheres, without the need to use light- or heat-sensitive materials to initiate a polymerization process. It has also been shown that droplet microfluidics can be used to form interesting morphologies. For example, tadpole-shaped Fe_3O_4-chitosan composite particles were prepared using a flow focusing device by Yang et al. [85] (Fig. 10a-b). In this system, a solution of chitosan, and a mixture of

$FeCl_2$ and $FeCl_3$ was injected into a sun flower seed oil stream to generate magnetic droplets (Fig. 10a). The droplets formed on-chip were solidified off-chip in a NaOH solution as soon as they exited the channel. The dimensions of the Fe_3O_4-chitosan composite particles can be controlled by varying Q_d. When Q_c was maintained at 0.5 mL min^{-1} and Q_d was varied from 0.02, 0.2 and 0.3 mL h^{-1}, composites were generated with respective length/diameter (D/L) ratios of 2.2, 2.1 and 1.9. SEM images of the composite particles confirmed the formation of tadpole-like structures (Fig. 10b). Mitoxantrone, serving as a model drug, was mixed with chitosan, $FeCl_2$ and $FeCl_3$ to generate composite particles. An assessment of the
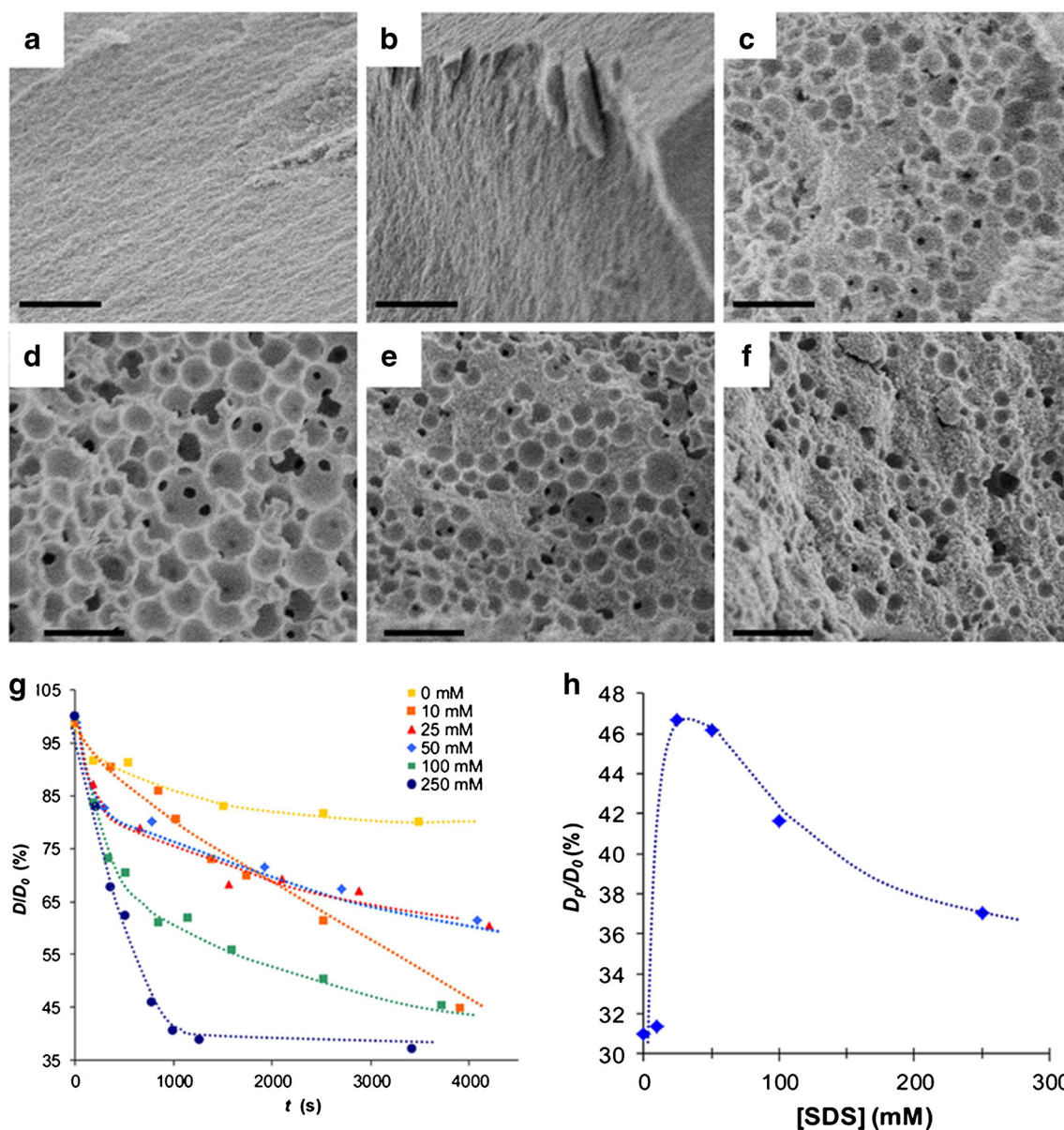
Fig. 9 SEM micrographs of the interior of the microspheres made from solutions of SPIONs and copolymer in toluene and collected in (**a**) 0, (**b**) 10, (**c**) 25, (**d**) 50, (**e**) 100 and (**f**) 250 mM SDS solutions (scale bar 1 μm). (**g**) Variation in droplet size as a function of time for droplets collected in

difference SDS concentration. (**h**) Changes in the porosity of particles as a function of the SDS concentration solution. Reprinted with permission from ref. [78]. Copyright (2012), American Chemical Society (ACS)

Fig. 10 **a**) A descriptive schematic of the microfluidic setup for the production of tadpole-like iron oxide-chitosan composite. **b**) SEM images of the formed tadpole-like composites prepared at $Q_d = 0.3$ mL h^{-1} and $Q_c = 0.02$ mL h^{-1}. Reprinted with permission from ref. [85]. Copyright 2014, Elsevier
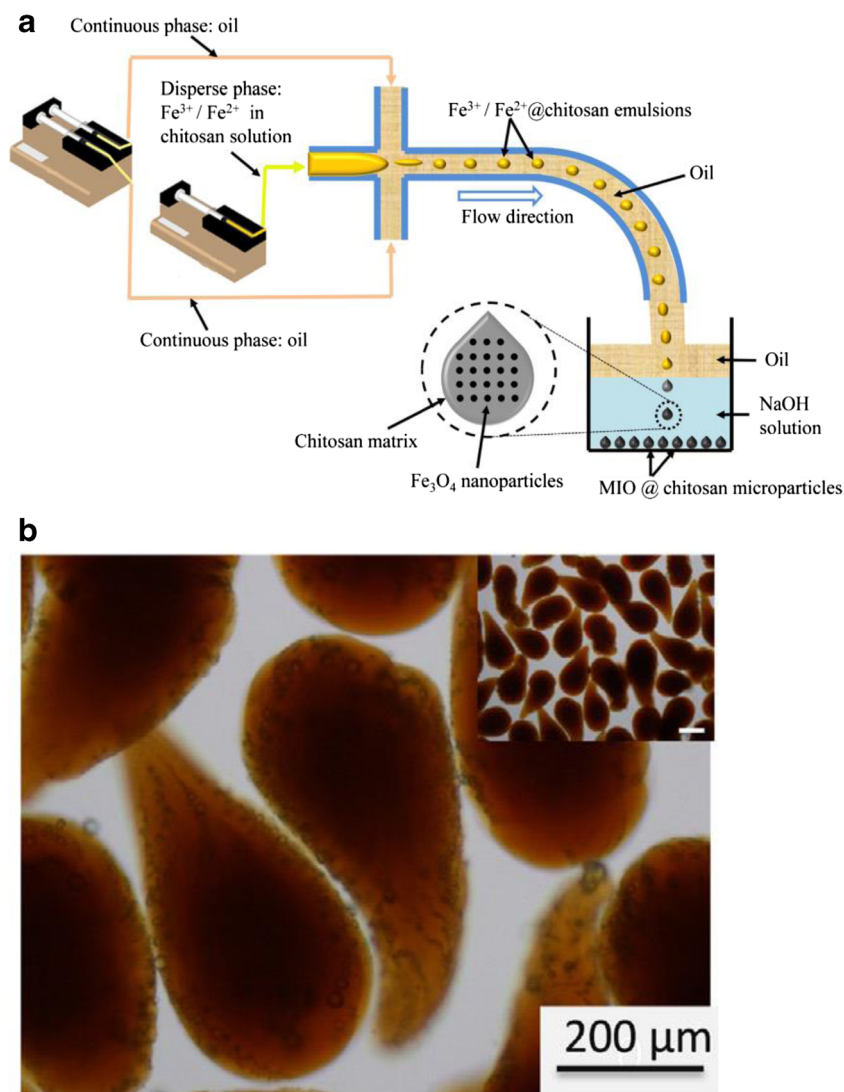
efficiency of drug release from the magnetic composite showed that the prepared composite had an encapsulation rate of 69% compared to 71% for the native chitosan particles. However, the magnetic composite displayed a larger drug release rate (41.6%) over 180 min compared to that for native chitosan (24.6%). The high efficiency of drug release rate was attributed to the increased porosity of the composites. Despite being able to generate this unique composite shape, the authors do not mention if this shape has any advantages over spherical or disk-shaped particles that can be prepared using droplet microfluidics. Additionally no in vivo study was conducted to probe the applicability of this method for encapsulation and release. Porous magnetic beads were prepared using droplet microfluidics for separating oil/organic solvent contaminants in water [86, 87]. A suspension of acidified multiwall carbon nanotubes (aMWCNTs), polystyrene (PS) microspheres and Fe$_3$O$_4$ NPs was used as the dispersed phase and dimethyl silicone oil as the continuous phase [86]. Porous

aMWCNTs are well-known adsorbents, while PS served as a hard and porous template for the droplets and Fe$_3$O$_4$ NPs enabled remote and wireless control of the beads after solidification. The droplets were collected off-chip and hardened at 60 °C for 12 h, washed and then heated at 750 °C for 2 h to form porous magnetic beads. The beads were characterized using SEM, Fourier-transform infrared spectroscopy (FTIR), X-ray powder diffraction (XRD), X-ray photon spectroscopy (XPS), surface area and Raman spectroscopy. After exposing the beads to oils or organic solvents, they can be isolated using an external magnet (Fig. 11a1-a6), and the adsorption can be monitored by digital imaging. In addition, the beads were recyclable using combustion and distillation approaches. A reduction by only 4.3% in their absorption capacity occured following their use for 6 cycles when using the combustion recovery approach and negligible loss recorded when using the distillation recovery protocol. No information was provided regarding the features (eg. quantities, and concentrations)

Fig. 11 Photographs of the adsorption process of pump oil (yellow) in water, the adsorption was completed within 40 s then the magnetic porous aMWCNTs were collected using a magnet. Reprinted with permission from ref. [86]. Copyright (20116), the Royal Society of Chemistry (RSC)
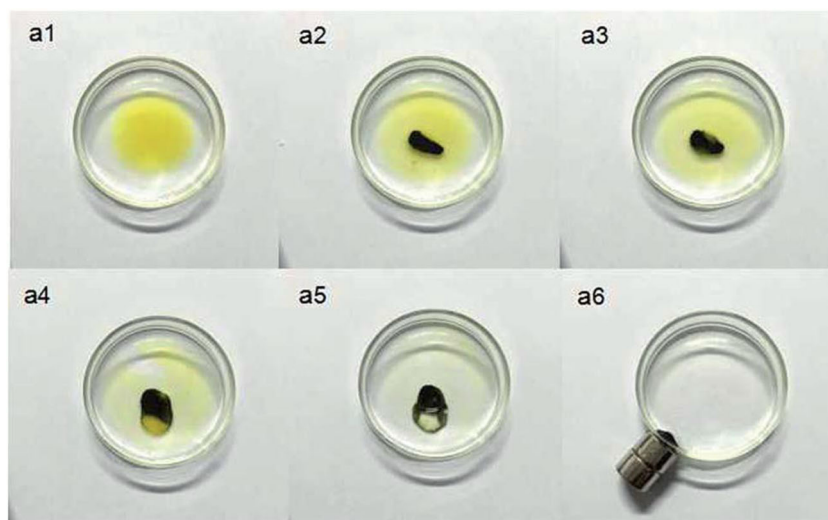
of oil/organic solvent removal. The same group described the use of the same strategy to generate magnetic porous graphene oxide/multi-walled carbon nanotube beads (MPGCBs) in the same capillary microdevice [87]. In this case, the beads were formed on-chip in a continuous flow mode by injecting a mixture of graphene oxide (GO), aMWCNTs, polystyrene beads (PS) and Fe_3O_4 NPs in dimethyl silicone oil. The GO/aMWCNTs/PS/ Fe_3O_4 droplets were collected and solidified in the manner described above to yield magnetic beads. The MPGCBs were characterized using SEM, FTIR, XRD, XPS, Raman and UV-Vis spectroscopy. The results of the XRD and XPS studies confirmed the magnetic properties of the formed beads, and the presence of iron, carbon and oxygen. The contaminant absorption capacity of the beads was assessed by exposing them to a series of oils/organic solvents. The results showed that the beads can absorb 8–25 times their own weight. By placing the MPGCBs between two Nylon filters, several water-in-oil emulsions can be separated, because the oil passed through the MPGCBs while the water was repelled by the hydrophobic MPGCBs and, thus, remained on the membrane surface. However, the authors did not mention the advantage of adding GO to the MPGCBs, nor did they carry out surface area measurements of the formed beads in order to obtain information about their adsorption behavior for comparison to previously described systems.

Conductive, pH-sensitive and thermoresponsive magnetic particles have been successfully generated using droplet microfluidics. In an initial effort, conductive and magnetic Fe_3O_4-poly(3,4-ethylenedioxythiophene) (PEDOT)/polystyrene sulfonate (PSS)-agarose polymeric microspheres were fabricated employing a flow focusing device [88]. The aqueous phase was prepared by off-chip mixing of a number of substances including PEDOT, PSS, PVA, agarose and Fe_3O_4 NPs. The mixture was then injected on-chip into a silicone oil stream. The droplets were collected off-chip in an ice bucket, solidified and repeatedly washed. As has been previously demonstrated in several studies, the size of the droplets (microspheres) depended on Q_c and Q_d, and in this study Q_c was varied at a fixed Q_d to optimize the particle size. The microspheres were characterized using scanning electron microscopy-energy dispersive X-ray spectroscopy (SEM-EDX), XPS and XRD, in order to evaluate the morphology and elemental composition of the microspheres, and VSM was utilized to measure their M_s. SEM images showed that the microspheres had a cracked surface and wrinkled morphology, which have been seen previously when MNPs were mixed with a polymer mixture. EDX, used for cross sectional examination of the microparticles, showed that a uniform distribution of Fe and S atoms were present inside the particles. In addition, XRD peak(s) appearing at $2\theta = 20°$ corresponded to PEDOT/PSS-agrose in the microparticles and those at $2\theta = 30.1°$, $35.4°$, $43.1°$, $53.5°$ and $56.9°$ corresponded to pure Fe_3O_4. On the other hand, no peaks for Fe_3O_4 were observed in the XPS, which was suggested to be a consequence of the presence of MNPs inside the microparticle rather than on the surface. However, XPS peaks at 708 and 711 eV in Fe_{2p} spectrum were seen when larger Fe_3O_4 particles were incorporated into the PEDOT/PSS-agrose microparticles. Due to the small content of the MNPs in the spheres (0.75% wt%), the M_s value was estimated using VSM to be 5.4 emu g^{-1}, which was lower than M_s values obtained for conventional core/shell PS beads. The electrical resistance of the microspheres was measured by fixing the particles on the surface of a glass slide in the form of a single layer using silver paste. The results showed that the addition of Fe_3O_4 NPs caused an increase in the resistance to 8.3×10^3 Ω in comparison to 85 Ω for the native microspheres. Furthermore, VSM was employed to measure M_s in order to determine the magnetic behavior of the fabricated microspheres. However, no applications were suggested for the material described in this investigation. Magnetic and

photoresponsive, ferrite NPs incorporated in epoxide-bearing graphene oxide (GO) microcapsules were first prepared by Kaufman et al. [89], In a single-step within droplet microfluidics. In the process, epoxide-bearing fluorescein isothiocyanate-GO (FITC-GO) reacted interfacially with amine functionalized macromolecular silicone oil (continuous phase) to generate a chemically cross-linked film with macro-scale thickness at the surface of the droplet-oil interface. The addition of the ferrite NPs (NiZn ferrite) enabled positioning of the droplets using an external magnetic field. Initially, aqueous FITC-GO droplets were formed in sizes ranging between 275 and 440 μm using no ferrite NPs in a simple T-junction device by varying Q_c and Q_d. The formed microcapsules were solid-like shells with wrinkled surfaces due to water loss by osmosis occurring when the capsules were collected. Then, microcapsules were generated using a double emulsion approach to form a W/O/W system. NaCl was used to avoid water loss and, thus, reduced surface wrinkles. The roles of GO and oil concentrations on the stability and morphology of the formed microcapsules were investigated. At a fixed oil concentration of 2.5% (wt%), the capsules were stable against merging at GO concentrations ranging from 0.1 to 5% (wt%). At an oil concentration of 5%, the GO capsules appeared non-spherical and had an opaque surface due to GO aggregation. The stability of the microcapsules was more sensitive to the oil concentration, where at low concentration coalescence was observed to occur due to low interfacial tension between the two phases. On the other hand, the presence of high polymer concentration caused a decrease in interfacial access thus preventing the buildup of sufficient GO to form a stable membrane. The thermal response of the microcapsules was investigated using methyl orange with GO and monitoring release of this dye from the capsules as a function of time. Without the use of near infrared (NIR) radiation, the capsules lost 25% of the dye in about 30 min. However, NIR radiation caused loss of ca. 90% of the dye. Capsules generated using a mixture of NiZn ferrite NPs and GO showed a significantly different behavior, including the coalescence between the droplets and formation of spherical and nonspherical capsules. The morphology of these capsules was also affected by the concentration of the NPs. For instance, the use of concentrations above 0.01 wt% led to generation of dumbbell- or peanut-shaped capsules as a consequence of the accumulation of NPs on GO sheets and obstruction of the reactive sites. Application of a magnetic field to the dumbbell-shaped capsules caused the location of the ferrite NPs to shift to one side of the capsule, leading to an interesting Janus particle-like structure. The formed capsules, having dual magnetic and photoresponsive properties, have the potential of being used in several practical applications. However, this investigation mainly focused on the microcapsules rather than their magnetic functionality and the applications of the prepared capsules were not explored. In another study, pH-sensitive

magnetic microspheres were prepared for treatment of colorectal cancer using a simple T-junction design [90]. The multifunctional microspheres had a narrow size distribution (CV >5%) and contained: anticancer drugs (5 fluorouracil (5FU) and curcumin (CUR) silicon nanoparticles (SiNPs) and bacterial magnetic nanowires (BacNWs) to enable guiding of the spheres inside the human body by using an external magnet. The drugs were loaded into the SiNPs and BacNWs, and mixed in a multi-step off-chip protocol in eppendorf tubes. This followed by on-chip generation of the uniform pH-sensitive polymeric microsphere of hypromellose acetate succinate (Fig. 12a-b). The microfluidic platform used in this effort provided control over microsphere size resulting in an average size of 26.5 ± 0.7 μm after solvent removal. Moreover, 10 min of exposure to a slightly basic solution (pH 7.4) disintegrated the sphere causing the release of its contents. The results of an in vitro biocompatibility test was performed using human RAW 264.7 microphages revealed that up to 1000 μg L^{-1} concentration of the spheres (no drugs loaded) did not result in toxicity to the microphages. Additionally, the synergistic effect on SW480 colon adenocarcinoma cells was assessed by incubating the cells with drug loaded microspheres. Combination indices (CI) of 0.58 and 0.73, were observed using respective 1:2 and 1:1 ratios of 5FU to CUR. Use of both ratios led to similar and significant levels cell death. The methodology developed in this effort can significantly reduce the amount of the drug used and, as a result, side effects. Although being significant to the field of drug delivery, the advantage of using BacNWs over magnetic particles was not highlighted, and the biocompatibility of the drug loaded microspheres was determined.

The principle of FFM was also employed to achieve layer-by-layer (LbL) deposition of polyelectrolytes (PE) of alternating charges on magnetic droplets for drug delivery purposes [57]. The oil-based FF droplets size was controlled by the channel dimensions, Q_c and Q_d. In this effort, different size oil-based FF droplets were generated by controlling Q_c and Q_d, and using 3 T-junctions or flow focusing designs including shallow, deep and snakes-and-ladders chips. The FF droplets were initially stabilized using the surface active polymer polyvinylpyrrolidone (PVP) and then were fed into a shallow flow chamber under the influence of the hydrodynamic flow. The chamber contained two parallel multi-laminar streams of PE, including cationic poly(fluorescein isothiocyanate allylamine hydrochloride) (PAH-FITC) and anionic poly(sodium-4-styrerne sulfonate) (PSS), and two streams for alternating washing with Tween 20 solution. Using a magnet placed at the opposite end of the chamber, the droplets were deflected across the chamber and passed through the laminar streams (Fig. 13a). In the shallow chip design (20 μm deep), the droplets were 'squashed' and stuck to the chamber walls, which led to their coalescence. The use of a deeper chamber design (100 μm deep) can overcome this

Fig. 12 Schematic illustration of **a**) T-junction geometry used to generate pH-sensitive and magnetic microspheres and **b**) microspheres containing bacterial nanowires, silicon NPs, and drugs. Reprinted with permission from ref. [90]. Copyright (2017), the Royal Society of Chemistry (RSC)
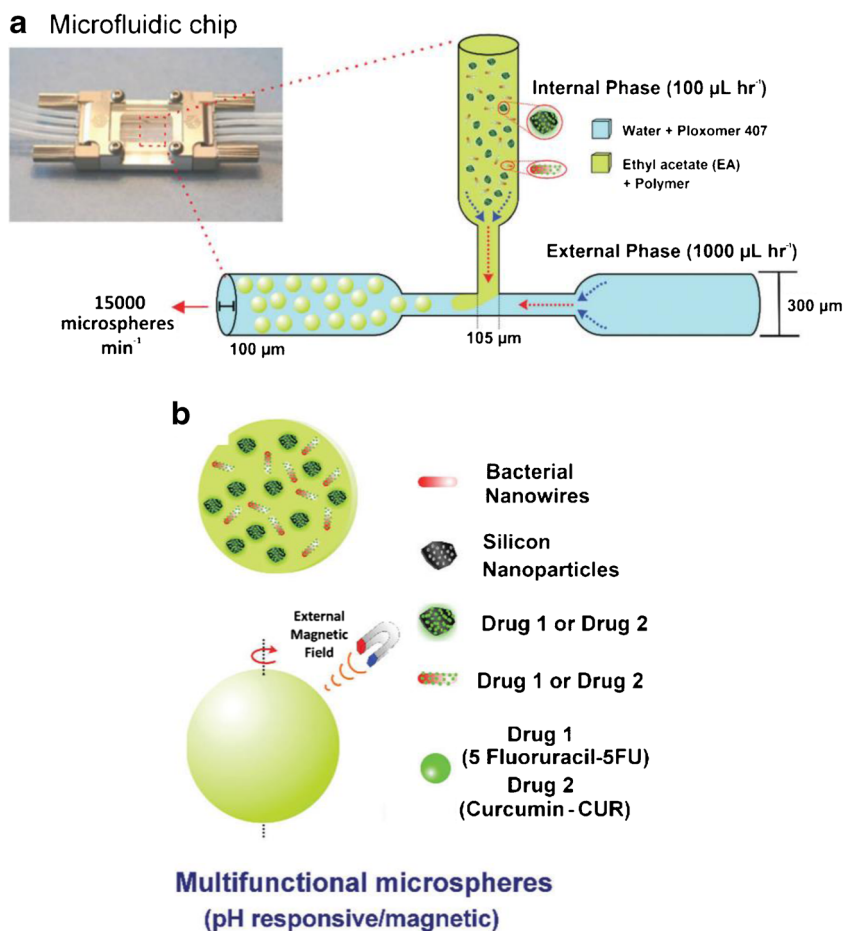
Fig. 13 a) Schematic of continuous flow LbL deposition of PEs using deflection of magnetic droplets through PE multi-laminar flow streams and washing solutions in the presence of the magnetic field. **b**) The "snakes-and-ladders" microfluidic design and principle of FF magnetic droplet deflection through PEs and washing streams in the presence of the magnetic field. Reprinted with permission from ref. [57]. Copyright (2017), The Royal Society of Chemistry (RSC)
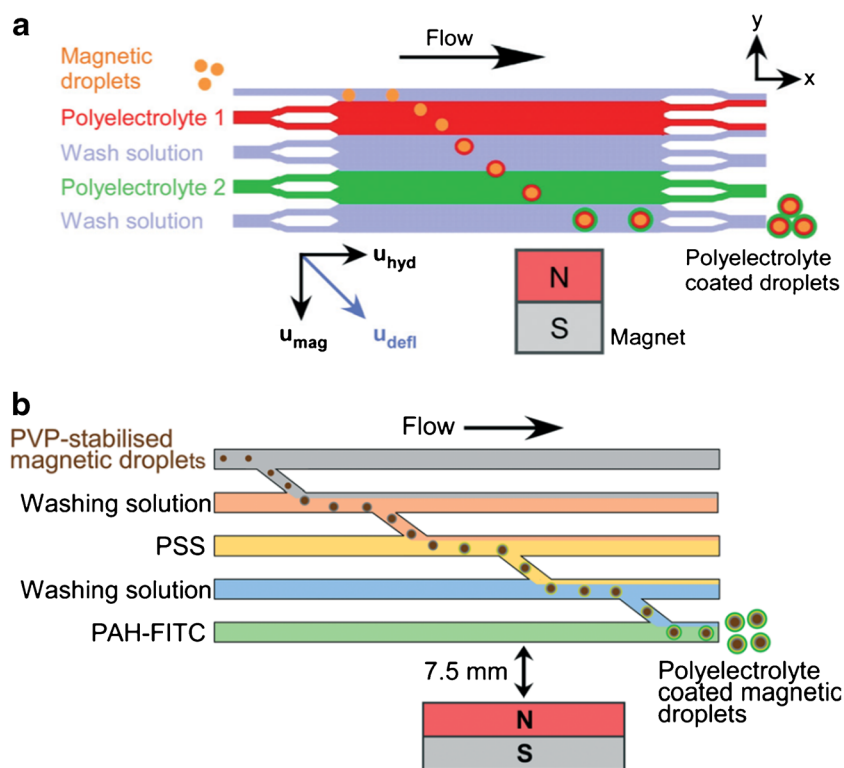
issue. However, although deflection across the laminar streams was successful, deposition of PE was challenging due to disturbance of the streams by external factors such as accidental microscope stage movement. Control of the droplet deflection trajectory and PE deposition was accomplished by utilizing a unique "snakes-and-ladders" chip design in (Fig. 13b). Although this design was practical and overcame issues encountered with use of the previous designs, no final washing steps were possible before the PE coated FF droplets were collected off-chip. Furthermore, the authors did not provide examples of drug encapsulation and delivery using the LbL PE droplets.

Synthesis of Janus magnetic particles

Janus photonic crystalline particles of SiO_2 and MNPs were first synthesized in 2013 using a glass capillary assembly [91]. The dispersed phase used in this process composed of a mixture of solutions of SiO_2 (200–300 nm) and Fe_3O_4 (12 nm) NPs, which merged into a silicone continuous phase to form water-in-oil droplets in the collection container. The collection procedure was performed off-chip and the droplets were subjected to an external magnetic field for 10 min to separate the two phases and form Janus particles. Then, the solvent was evaporated followed by washing the solid particles with hexane to remove residual oil. The optimized volume ratio of SiO_2 to Fe_3O_4 NPs was around 70:1, which contrast with the previously reported value of 7.7:1, the latter being attributed to the escape of NPs from the droplet template.

Inspection of SEM images showed that although the SiO_2 NPs were hexagonally aligned on the surface of Janus particles, the presence of Fe_3O_4 NPs distorted this alignment at some locations. Additionally, the findings showed that when 220, 260 and 290 nm SiO_2 NPs were used, a range of Janus particles with different reflection peaks at 480, 570 and 640 nm, respectively, were produced (Fig. 14a-d). Furthermore, a DNA hybridization assay was performed on the produced Janus particles. For this purpose, the Janus particles were used as carriers for oligonucleotides, mixed with fluorescently labeled oligonucleotides and incubated for 20 min using rotational motion, which was found to improve the fluorescent signal. Another capillary assembly system was devised for the synthesis of half polymeric and half magnetic Janus microparticles by Yang et al. [92]. The two polymerizable dispersed phases were used in this approach to fabricate Janus particles include dispersed phase I containing tri(propyleneglycol) diacrylate and 1-hydroxycyclohexyl phenyl ketone (as photoinitiator), and dispersed phase II containing kerosene, 4–6%(methacryloxypropyl) methylsiloxne-dimethylsiloxane copolymer, 1-hydroxycyclohexyl phenyl ketone (as photoinitiator) and the synthesized MNPs. Upon merging with the continuous phase of aqueous sodium carboxymethyl cellulose (CMC), a meniscus containing the two dispersed phases was formed and broke up to produce Janus droplets, which were monitored by using optical microscopy. Further downstream, the droplets were exposed to UV light to promote the consolidation of the Janus particles. Due to the limitation associated with the inner diameter of the


Fig. 14 a–c) Reflection light images of three types of Janus particles of different SiO_2 NPs sizes (220, 260 and 290 nm). d) Reflection spectra recorded for the quantum dots and magnetic Janus particles. Reprinted with permission from ref. [91]. Copyright (2013), the Royal Society of Chemistry (RSC)
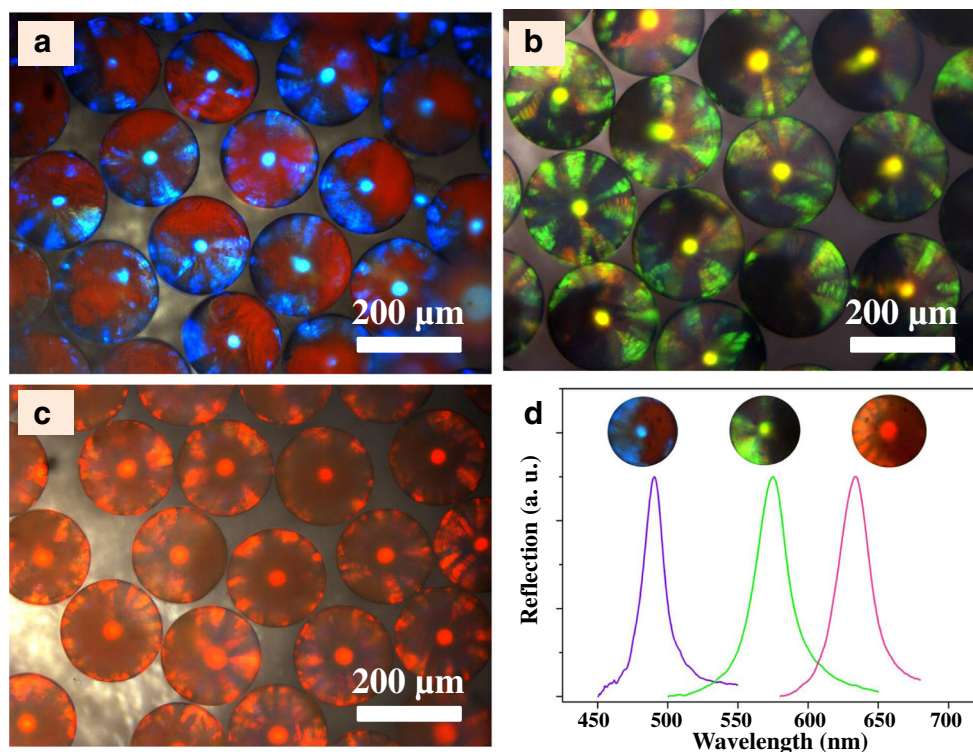
capillaries and maximum speed of the syringe pump, a flow focusing design was employed instead to generate Janus droplets of smaller sizes. Using this protocol, manipulation of both flow rates generated Janus particles with overall sizes ranging from 200 to 800 μm and with different volume fractions in the segments. A magnetic orientation experiment was performed in which the particles were suspended in CMC solution and exposed to an external magnetic field. Upon exposure to the field, the synthesized Janus particles rotated at a speed of 6.5° s^{-1}, showing they are good candidates for biomedical applications such as drug delivery. Magnetic and fluorescent Janus microparticles based on CdSe/ZnS quantum dots (QDs) and Fe_3O_4 NPs (particle size not identified) were synthesized using droplet microfluidic technique [93]. In the process, a dispersed phase I consisting of alginate solution (4.0% wt:wt) and carboxyl modified CdSe/ZnS aqueous QDs was pumped through the first inlet, while dispersed phase II containing Fe_3O_4 NPs in alginate solution (4.0% wt:wt) was introduced through a second inlet. Both solutions moved through a Y-channel and merged with the continuous phase comprised of $CaCl_2$ and oleic acid at a flow focusing orifice to form droplets, which eventually solidified at a serpentine mixing channel due to diffusion of Ca^{2+} from the oil phase into the droplet forming Ca^{2+}/sodium alginate crosslinks. The viscosity of the alginate solution and velocities of the fluids were varied to optimize generation microparticles having different magnetic/fluorescent contents. Fluorescence microscope images of the magnetic/fluorescent Janus microparticles, produced using different QDs, show that both Fe_3O_4 NPs and QDs maintained their spatial positions in the two hemispheres of the microparticles and, as a result no quenching of fluorescence by Fe_3O_4 occurred (Fig. 15a–d). The magnetic/fluorescent Janus microparticles were used to perform a DNA assay in which the target DNA was captured on the Janus microparticles and incubated overnight at room temperature. A reporter DNA modified with FITC was then hybridized with the target DNA on the conjugated microparticles,

which were then incubated for 30 min at room temperature. After hybridization was completed magnetic separation was performed and positive detection was carried out using fluorescence microscopy. Although the approach is very interesting, fluorescent QDs did not play a direct role in the assay. Another magnetic/fluorescent Janus particle platform was generated by using a high flow, surfactant free and wash-less method, which combining droplet micro-magnetofluidics (DMMF) and hybrid magnetic fields [79]. The device had a flow focusing design, in which the dispersed phase was composed of co-flowing streams of magnetic polymeric phase (MP) and polymeric phase (PP). The droplets were formed downstream and exposed to a hybrid magnetic field (400 mT) and then UV light. Based on the results of Ca calculations, droplet generation was governed by a squeezing regime (Ca < 10^{-3}). The simulated and experimental Janus droplet sizes as a function of Q_c/Q_d were found to be in agreement. Control of the Janus droplets was investigated as the droplets traveled through the hybrid magnetic field. At a distance of 0 mm, the magnetic field caused the MNPs to form chains along the y-direction, and at flow rate ratios less than 7.5 more chains were formed due to the dominance of the magnetic over the hydrodynamic force. At a distance of 13 mm and low flow ratios (2.5 and 5), the magnetic force caused the MNPs to concentrate on one side of the droplet, where they subsequently solidify upon exposure to UV light. The generated Janus particles were characterized using optical microscopy, VSM, FTIR, differential scanning calorimetry (DSC) and thermogravemtric analysis (TGA). Optical images showed that Janus particles formed using this technique, and VSM data showed that the particles display magnetic behavior with a coercivity of 4–10 Oe. Characteristic bands in the FTIR spectrum of the particles indicated that successful polymer formation has occurred and DSC analysis proved superior polymerization occured at low flow rates. TGA showed that the Janus particles displayed a higher weight loss compared to that of pure MNPs, which was attributed to the presence of a

Fig. 15 Bright field and fluorescence images of Janus microparticles containing Fe_3O_4 NPs and three types of QDs at emission wavelengths of a) 525 nm (green), b) 585 nm (yellow) and c) 625 nm (red). Reprinted with permission from ref. [93]. Copyright (2015), Elsevier
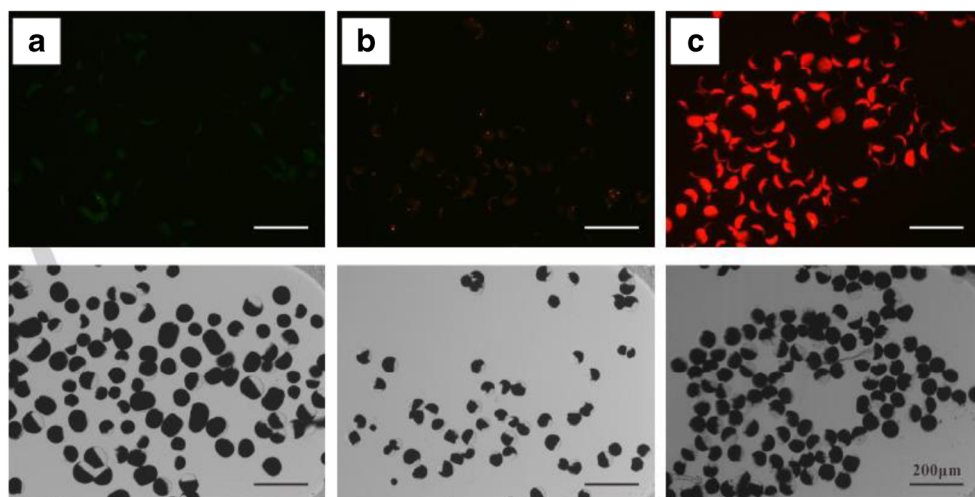
hybrid magnetic field. Furthermore, the prepared particles were used to perform a protein detection assay employing flourescein isothiocyanate-bovine serum albumin (FITC-BSA) as a model protein. Covalent immobilization of FITC-BSA to the Janus particles was performed by ethyl(dimethylaminopropyl) carbodiimide (EDC) and N-hydroxysuccinimide (NHS) coupling. Inspection of fluorescence images of the Janus particles bonded to the FTIC-BSA showed that the use of increasing concentrations (20–200 μg mL^{-1}) of FITC-BSA led to increase in fluorescence intensity. Thus, the particles can be used to perform assays that are typically carried out in a 96 well plate. Finally, Yu et al. [94] synthesized multiferroic Janus microparticles using a 'face-to-face' bonded 'two-layer' PDMS device. In the system, two dispersed phase streams flowed on top of each other, rather than side-by-side, to form disk-like Janus droplets. The 'upper' and 'lower' streams were comprised of the ferroelectric polymer poly(vinylidene fluoride-trifluoroethylene) [P(VDF-TrFE)] and a suspension of Fe_3O_4 ferromagnetic NPs, respectively. Monitoring of the mixing the two streams, also supported with simulations, showed that negligible mixing occurs as the droplets moved 1–2.5 cm away from the generation point, while at further distances (eg., 7 cm) some mixing occurred, which was evidenced in SEM images. The microparticles were characterized using XRD, VSM and electric polarization. The XRD pattern contained diffraction peaks related to the presence in the particles of [P(VDF-TrFE)], Fe_3O_4 NPs and the initiator. Analysis of the VSM hysteresis loop confirmed the soft ferromagnetic nature of the formed Janus microparticles compared to those of the native polymer and Fe_3O_4 NPs. The ferroelectric property of the Janus microparticles was assessed by depositing the dried microparticles on the surface of gold point electrodes. Moreover, the ferroelectric curve of polarization vs. the applied electric field was found to exhibit ferroelectric character with a remnant polarization value of 15.1 μC cm^{-1} due to the presence of [P(VDF-TrFE)]. These results proved that the microparticles had dual ferromagnetic and ferroelectric properties. It is claimed that the shape of the microparticles was disk-like rather than spherical and that because of this unusual geometry they were more stable than particles obtained by using conventional methods. Moreover, single phase instead of Janus particles can be produced using the same setup by mixing the two streams prior to UV exposure and solidification of the particles. This great development in the fabrication of magnetic Janus particles using droplet microfluidics will hopefully inspire future work in areas of biosensing, coatings, drug delivery and others.

Synthesis of magnetic hydrogel particles

The synthesis of magnetic hydrogel particles via UV polymerization was first demonstrated by Hwang et al. [95]. This study explored the generation of spherical magnetic hydrogels, deformed disks as well as plugs, in continuous flow utilizing a T-junction design. In the system, two immiscible phases were independently controlled by using air pressure. The different hydrogel morphologies were obtained by varying the pressures of the dispersed (P_m) and continuous (P_0) phases. For example, at $P_m = 20.7$ kPa and $P_0 = 31.7$ kPa deformed spheres were produced, and uniform spheres were generated at $P_m = 33.1$ kPa and $P_0 = 52.4$ kPa. In addition, disks were formed at $P_m = 5.5$ kPa and $P_0 = 12.4$ kPa and finally plugs were produced at $P_m = 31.7$ kPa and $P_0 = 46.9$ kPa. Hydrogels with all of these morphologies exhibited high monodispersity with CVs less than 2%. The hydrogel particles displayed superparamagnetic behavior as determined by using VSM measurements and they can potentially be used in biological applications due to their biocompatibility. Another synthesis platform probed is based on a PDMS device comprised of two flow focusing configurations, which produces double emulsion magnetic droplets [28]. The droplets consisted of a magnetic hydrophobic core encapsulated by a hydrophilic monomer droplet, which was then suspended in fluorocarbon-based oil. The double emulsion was collected in a container and solidified by exposure to UV-light for 10 min. The spherical magnetic gel particles, following being washed, dried, and re-dispersed in water, contained either one or two magnetic cores based on the experimental conditions used for their production (for more details see ref. [28]). When the volatile fluorocarbon oil and water were removed by evaporation, the magnetic particles became more compact and exhibited uniform an anisotropic morphology, in that the particles rotate eccentrically around a point in the magnetic core. Despite their unique properties, very few investigations have focused on these magnetic hydrogel particles. Thus, it remains to be determined if magnetic hydrogles with different swell/shrink ratios, degree of crosslinking, sizes and surface charges can be fabricated in microfluidic devices for applications in the areas of cosmetics, personal care and food.

Assay-based continuous magnetic droplets applications

Compartmentalization of reagents within a single droplet minimizes contamination and dilution effects, therefore, they can be used for carrying out isolated multiple bioassays simultaneously. Additionally, the incubation time of samples in droplets can be increased by lengthening the channels or collecting the droplets in a container [26]. Therefore, magnetic droplets have been utilized to perform biological assays, including measuring binding of drugs to proteins [19], immunoassays [41] and DNA-based assays [96]. Detection in these assays has been achieved mostly by using optical methods such as

fluorescence due to its high sensitivity and ease of integration with the microfluidics technology. The different detection methods employed in various assays based magnetic droplets are summarized in Table 7. In one example, the continuous generation and processing of nL magnetic droplets has been used to determine the binding constant (K_A) of warfarin to human serum albumin (HSA) [19]. In this system, magnetic beads (MB) are coated off-chip with human serum albumin (HSA) to form HSA-MB, and then mixed with warfarin before being injected into a stream of oil at a T-junction. The droplets were then split at another T-junction using an external magnetic field in a manner that is similar to one reported previously [18]. Around 95% of the magnetic beads can be collected when the beads concentration was 3.3 mg mL^{-1} and 100% were collected when lower concentrations (<1 mg mL^{-1}) were utilized. Loss in the efficiency of bead isolation occurred when a weak magnetic field was applied and when high flow rates (>5 μL min^{-1}) and large magnetic bead concentration (50 mg mL^{-1}) were used. Measurements of free and bound warfarin concentrations in the daughter droplets enabled the determination of K_A. The results showed that the ratio of concentrations of bound and free warfarin was 1.59 ± 0.291, independent of the initial concentrations used. Based on the data, K_A was determined to be $4.74 \pm 2.84 \times 10^5$ M^{-1} with the large standard deviation being attributed to the inconsistency in the concentration of HSA immobilized on the magnetic beads. The authors pointed out that the system can be utilized in other applications, such as binding assays, kinetic studies and single cell analysis [19]. Using a similar approach, Lee and co-workers [26] developed a novel microfluidic chip based system for manipulation of magnetic droplets that combines electrostatic and magnetic forces. The platform was used to perform robust immunoassays based on the streptavidin-biotin reaction coupled with fluorescence detection. The flow focusing device used in these assays was comprised of two parts including electrodes to achieve electrocoalescence of the droplets and a stationary magnet to accomplish magnetic-bead separation prior to their split at a T-junction. The first step in the process involved charging the solution streams, including stream 1 containing streptavidin-magnetic beads suspended in water and stream 2 containing fluorescently labeled biotin by using needles and an electric field with a voltage of 20 V. This charging caused attraction between the streams at the location of droplet generation where coalescence took place and it enabled control of coalescence by simply switching the field "on" and "off". The droplets then travelled in a winding channel to ensure homogenization of the droplet contents. Subsequent to mixing, the droplets approached a T-junction where they split into two daughter droplets. The magnetic field was applied near the junction to concentrate the magnetic particles into one of the daughter droplets, as has been previously demonstrated by other authors [18, 19]. The separation working zone for isolation of the magnetic droplets was influenced by the total flow rate ($Q_c + Q_d$ up to 500 μL h^{-1}) and the position of the magnet. Increasing the distance between the magnet and the channel caused an exponential decrease in the magnetic field strength. Optimum isolation of the beads was achieved using a $Q_c + Q_d$ of 400 μL h^{-1} and a distance of 1 mm. The assay was actually performed at $Q_c = 60$ μL h^{-1} and $Q_d = 30$ μL h^{-1} in order to produce an average droplet size of 120–125 μL for ideal fluorescence imaging. The authors reported that occasional merging of the daughter droplets took place at the outlets, giving a < 0.5% error rate that can be avoided by using a surfactant or maintaining a suitable distance between the droplets by controlling $Q_c + Q_d$ [26]. A capillary-based platform containing integrated multiple magnetic tweezers to manipulate magnetic droplets with downstream fluorescence detection was developed by Ali-Cherif et al. [41]. The magnetic tweezers in this device were made comprised of two sharp magnetic tips facing each other across a capillary, with each tip having the capability of being independently activated. As the magnetic droplet (80 nL) approached the tweezers tips, the particles inside were attracted to one of the tips and formed a cluster

Table 7 A summary of methods used for assays performed in magnetic droplets

Microfluidic system	Analyte(s)/immunoassay	Detection mode	Reference
Fused silica capillaries	Single cell DNA purification of human lung carcinoma (A549) cells and enzyme activity assay of β-galactosidase in rat phenchromoctoma (PC12) cells	Fluorescence	[98]
PDMS	Warfarin-HSA binding assay	Fluorescence	[19]
PDMS	Biotin-streptavidin binding assay	Fluorescence	[26]
PDMS	Diagnosis of prostate cancer (prostate-specific antigen (PSA))	SERS	[97]
PDMS	Cell culture of Hela and HEK293 cells	Fluorescence	[101]
Two PDMS devices, pipetting capillary, 384-wells MTP and PTFE capillary	Diagnosis of breast cancer using SKBR3 and MCF7 cell lines	SmartCycler analyzer	[96]
Teflon tubing	Diagnosis of neonatal congenital hypothyroidism (CH)	Fluorescence	[41]
Teflon tubing	Immune-agglutination assay of biotinylated phosphatase alkaline	Bright field microscopy	[100]

resulting in droplet deformation. As long as the magnetic force surpassed the interfacial forces, the droplets split into one small magnetic droplet (ca. 1 nL) and another non-magnetic droplet. The magnetic droplet was immobilized by the tweezers and merged with the upcoming droplet and the particles were re-dispersed. A determination of the degree of extraction of the magnetic particles from the droplet as a function of the flow rate showed that the flow rate had a minimal effect owing to the small droplet volume. A sandwich immunoassay for the diagnosis of neonatal congenital hypothyroidism (CH) was performed on a magnetic particle surface generated using this droplet system at room temperature (conventional assays are performed at 37 °C). An increase in the concentration of the thyroid-stimulating hormone (TSH > 30 mIU L^{-1} serum) is commonly used for this diagnosis. In the assay system, anti-TSH-magnetic beads containing droplet were first merged and incubated with TSH in a horse serum droplet. Trapped in the same tweezers, the magnetic beads with the antibody complex were washed with a third droplet containing a buffer to remove any non-specific adsorbed proteins. A fourth droplet containing enzyme-labeled secondary antibody was then merged into the complex containing droplet. After incubation, washing was performed to remove un-reacted secondary antibodies by merging with three buffer droplets. Finally, the particles were released and trapped at the last pair of magnetic tweezers for incubation with fluorogenic enzymatic substrate. A calibration plot was constructed for assay of 0–60 mIU L^{-1} of TSH concentrations in serum using fluorescence detection. The detection limit reported for TSH was 5.7 mIU L^{-1} (the cut-off limit is 30 mIU L^{-1}). The designed magnetic tweezers platform enabled particle exchange between the droplets with less than 2% carryover of the supernatant and a 98.9 ± 0.2% extraction efficiency. In addition, the droplet immunoassay was performed in 10 min compared to the 2.5 h time required using a conventional Immunometrics ELISA kit. Using the magnetic particle concentration concept, Gao et al. [97] designed a wash-free, automated, on-chip surface enhanced Raman spectroscopy (SERS) based assay for the detection of prostate-specific antigen (PSA). The microfluidic device was composed of droplet generation, mixing, splitting and detection regions (Fig. 16). The droplets contained a mixture of antibody coated magnetic beads, PSA and malachite green isothiocyanate gold NPs (MGITC-Au NPs), where MGITS served as a SERS nanotag. In this sandwich type assay, Au labeled PSA bound to the antibody on the surface of the magnetic beads. The resulting droplets then passed through a mixing zone composed of a serpentine channel. A permanent magnetic bar was present next to the channel wall to concentrate the magnetic droplets to one side while un-reacted (non-magnetic) droplets became located away from the magnet. Due to the hydrodynamic flow, the droplets separated at a Y-shaped junction and the non-magnetic daughter droplet flowed to a separate exit. Inspection of TEM images of

surfaces of the magnetic particles in the absence and presence of PSA antigen show that in the absence of the antigens no nanotags were bound to the particle surfaces. On the contrary, in the presence of the antigen, nanotags were present on the surfaces of the particles. The SERS signal was measured at the channel in which the magnetic droplets traveled using a Raman microscope coupled with a CCD camera. The intensity of the SERS signal depended on the Q_d/Q_c ratio with an optimum ratio being 1:7. The SERS measurement was carried out on-chip at a high flow rate of 174 droplet min^{-1}. A clear difference existed in the scattering spectra of the magnetic and non-magnetic droplets at the characteristic SERS nanotag peak at 1612 cm^{-1}, which can be used to quantitatively assess the concentration of PSA. Additionally, the limit of detection of the assay was found to be less than 0.1 ng mL^{-1} (no exact value was given), which was below the clinical cutoff limit (4 ng mL^{-1}).

The feasibility of using automated generation and manipulation of pL magnetic droplets for DNA purification at the single-cell level was reported by Gu et al. [98]. The user-friendly, DropLab platform (fabrication has been described elsewhere [99]) enabled solid-phase extraction and droplet splitting based on magnetic actuation. In this system, a group of sequential 500 pL droplets was generated inside a fused-silica capillary containing ferromagnetic particles in droplet 1, cells with magnetic beads in droplet 2, washing buffer in droplets 3 and 4, and elution buffer in droplet 5. The droplets were stationary in the capillary (250 μm i.d.), and were manipulated via the application of an external magnetic field. After DNA was released from the cell it bound to the magnetic beads which were suspended in the same droplet. The ferromagnetic particles present in the adjacent droplet were extracted in the form of small 10 nL magnetic droplets using a magnet and the formed mini-droplets merged with the droplet containing the DNA-bead complex. Droplet splitting was made efficient by the fact that the hydrophilic ferromagnetic particles promoted the passage of the magnetic beads through the phase orifice. The ferromagnetic particle/DNA-magnetic-bead cluster was then extracted by the magnet and merged with the buffer droplets to remove cell debris, proteins and lipids. The DNA-in-elution-buffer droplet can be recovered for further analysis (eg., PCR amplification). This platform was used to analyze single human lung carcinoma (A549) cells. The DNA recovered from the final droplet was purified, fragmented with 295-bp from human β-actin genes, amplified and analyzed using gel electrophoresis. Amplified DNA products were detected in 28 out of a total of 50 sample droplets, which indicated that the probability of positive results using the magnetic droplet system was ca. 56%. Moreover, multi-step manipulations including cell lysis, binding and release of DNA can be achieved in 5 min using this system [98]. Teste et al. [100] developed a fully automated and low-cost system for analyte detection that is based on a combination of
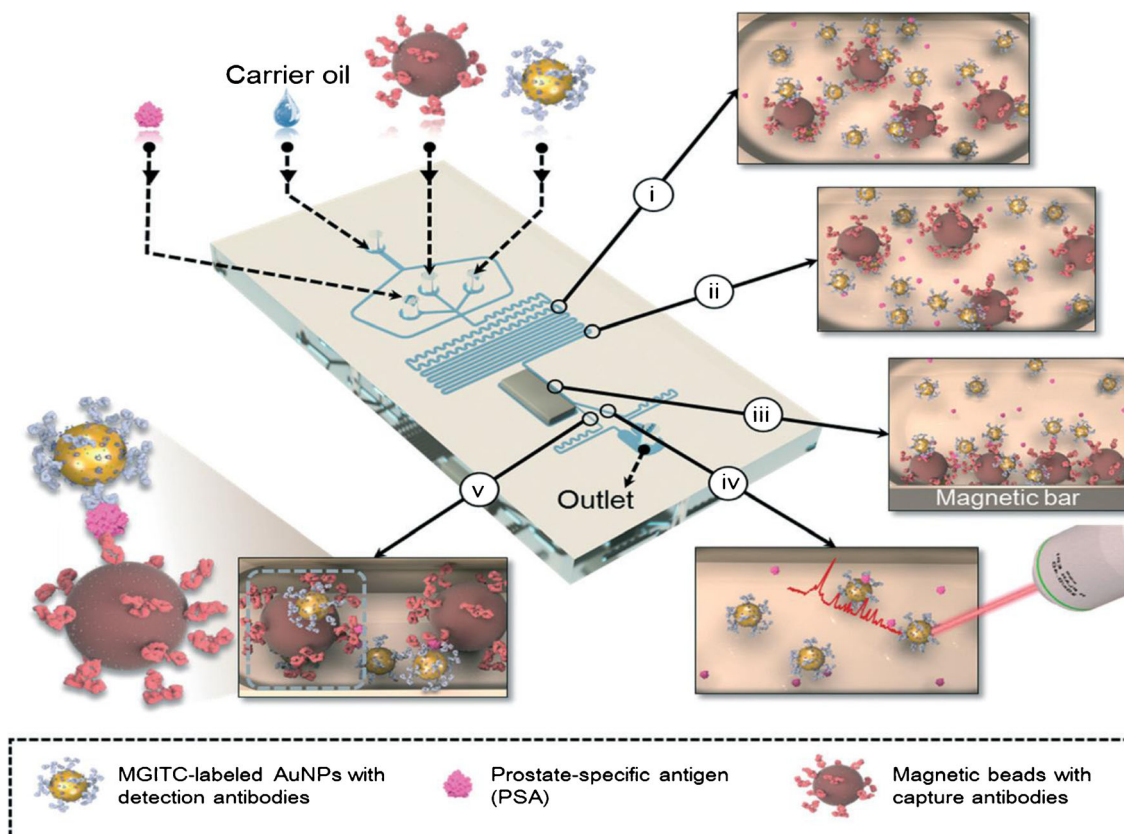
Fig. 16 Schematic illustration of the SERS-based microdroplet sensor. The main components of the platform are (i) droplet generation and reagent mixing, (ii) formation of magnetic complexes, (iii) isolation of the magnetic complexes, (iv) generation of larger droplets for SERS detection and (v) generation of smaller droplets containing reacted magnetic complexes. Reprinted with permission from ref. [97]. Copyright (2016), the Royal Society of Chemistry (RSC)

droplets, magnetic beads (MBs) and magnetic tweezers generated in Teflon tubing. Initially, streptavidin coated MBs were used to capture the biotinylated alkaline phosphatase. W/O droplets were first generated using an aspirating tip, the droplet contained the MBs and the analyte and was then transported in the tubing. A cluster of MBs within the group of moving droplets are affected by the external magnetic tweezers that enhanced the rate of agglutination. As the droplets moved away from the tweezers, an internal recirculation flow induced shear forces that caused redispersion of the MBs within the droplet. The analyte was then detected in the form of an observable optical contrast induced by the aggregates images obtained using the transmission mode. The findings demonstrated that the analyte in the system preserved its specific interactions and the MBs maintained an aggregated state (decrease from 70% to 28%). However, as the concentration of the analyte was reduced, the number of MBs participating in cluster formation and their binding strength decreased causing redisperion of the MBs in the droplet (Fig. 17I (A-F)). Several parameters that might influence agglutination process, such as magnetic field intensity, flow rate and MBs concentration, were optimized. The results showed that low flow rates caused the internal circulation to be insufficient to

redisperse the particles in the droplets. Additionally, the sensitivity of the assay was found to be low at high magnetic bead concentrations and the numbers of beads decreased as the numbers of captured molecules per magnetic bead increased. A calibration plot was generated with dynamic ranges of 100–900, 200–1100 and 500–1700 pM using 1, 2, and 3 mg mL^{-1} of magnetic beads (Fig. 17II). Finally, this magnetic droplet based agglutination assay has a high throughput and low cost. Magnetic droplets and magnetic tweezers were utilized in a fully programmed platform for RNA purification, reverse transcription (RT) and amplification using 250 nL droplets in a microtiter-plate [96]. Although the principle of operation of this system is simple, the experimental setup was somewhat complex. The main components of the system were a motorized pipetting arm for direct sampling of reagents from standard microtiter plates (MTP), magnetic tweezers to capture functionalized magnetic beads (used to capture and purify mRNA in samples) and transfer them between droplets, and a thermocycler in which RT and pre-amplification PCR cycles were carried out inside the droplets. However, the detailed setup illustrated in Fig. 18a–d includes droplet generation, an MTP placed under a motorized pipettor, two syringes, two pinch valves (V1 and V2), and two PDMS devices. In

Fig. 17 I) Bright field micrographs of MBs agglutination in droplets at 0 (A, B, C) and 2 nM (D, E, F) of the analyte before, during and after magnetic confinement. II) Calibration plots for immune-agglutination within the droplets using 1, 2, and 3 mg mL^{-1} of magnetic beads with dynamic ranges 100–900, 200–1100 and 500–1700 pM. Reprinted with permission from ref. [100]. Copyright (2013), the Royal Society of Chemistry (RSC)
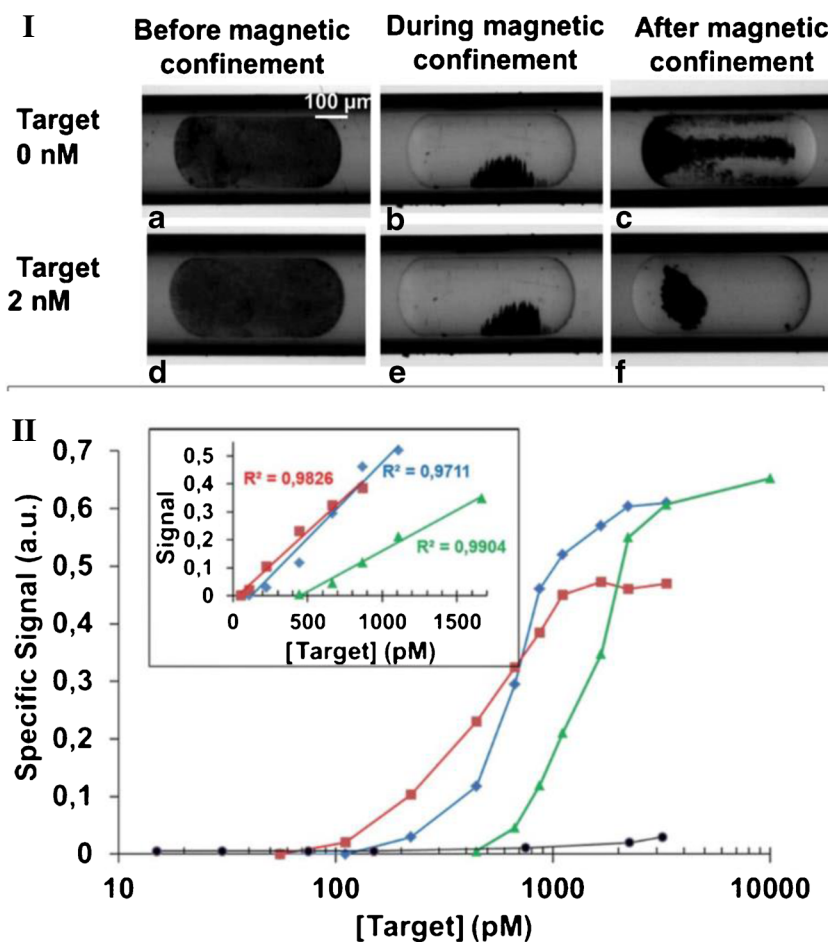
order to reduce the risk of contamination, a series of droplets containing reagents and the sample were loaded sequentially and travel a specified distance from each other inside a capillary. Two genes, reference gene TBP (TATA-binding protein) and HER2 (theranostic biomarker for breast cancer), were utilized in this study. TBP has a low variability of expression in cancer cells and was used to validate the quality of total RNA samples. The RNA was extracted from the cancer cells lines MCF7 (has normal levels of HER2) and SKBR3 (has HER2+, overexpressed gene). Calibration plots for the two genes were generated using quantities of total RNA ranging from 1.5 ng drop^{-1}-15 pg drop^{-1}, which were lower concentrations than those commonly used in clinical samples. Clinical validation was performed on RNA extracted from breast cancer samples using classical RT-qPCR at the hospital and by the droplet system in the laboratory. The results showed that both normal and overexpressed HER2 can be identified. The system enabled analysis of one sample every 3 min and 500 samples per day. A droplet-based microfluidic platform for encapsulation of cells and MNPs within 170–190 μm alginate beads, acting to mimic the function of multicellular tumor spheroids, was reported by Yoon et al. [101]. The system eliminated the need for tedious steps, such as

collection and transfer of the spheroids, by enabling maneuvering the spheroids were produced at a high rate of 200 spheroid min^{-1} using a magnetic field. The droplets in the system contained 4% CaCl$_2$, DMEM (medium), cells, MNPs and 0.5% sodium alginate. The platform consisted of compartments for droplet generation and separation. The gelled droplets (i.e. beads) were introduced into a channel which contained parallel flowing streams of oil and DMEM that were exposed to a magnetic field as they traveled down the channel. The magnetic force pulled the gelled droplets from the oil stream (toxic environment) into the medium stream. The alginate gelled beads were collected off-chip and examined using a fluorescence microscope. The beads were determined to have an average size of 184 μm after a 3 days generation period. Gelled beads containing spheroids were grown in a standard growth medium for 5 days. The cells appeared denser and more compact indicating that nutrients successfully diffused into the cells through the gelled alginate. Furthermore, to investigate the direct cell-to-cell connection, after 3 days of culture, the cells were chemically stained for visualization. The results showed that no empty gaps existed between the cells. An assessment of the ability of the spheroids to differentiate into a specific lineage was carried out by
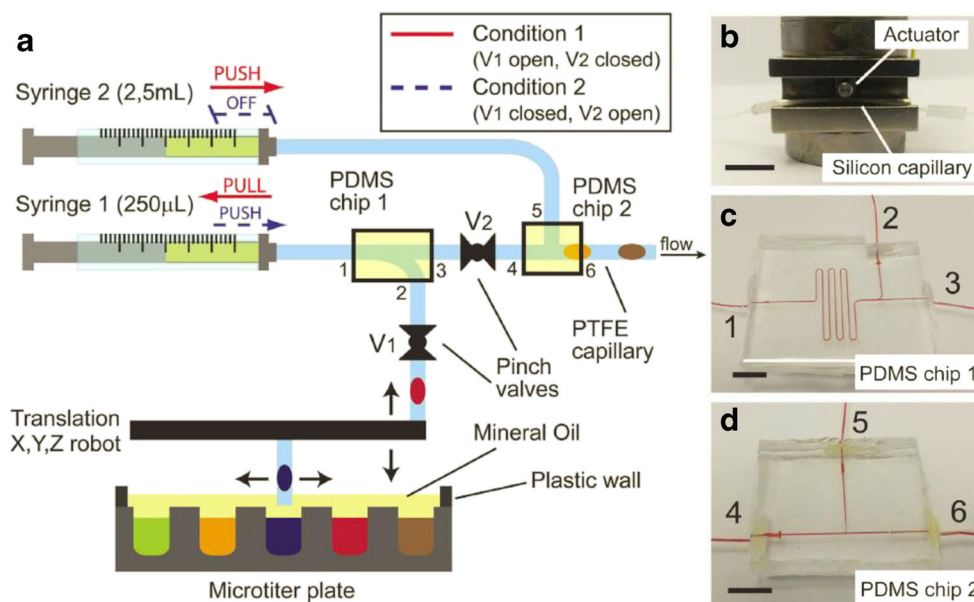
Fig. 18 Mircofluidic platform for the generation of a train of droplets for RNA purification, reverse transcription (RT) and amplification. (**a**) a schematic representation of the microfluidic platform showing the MTP plate and the automated pipettor, two syringes, two pinch valves (V1 and V2) and two PDMS devices. Syringe 1 is connected to inlet 1 of chip 1 (see part c of the figure), syringe 2 is connected to chip 2 (see part d of the figure) using a tubing passing through V1 and V2. Inlet 6 is connected to a capillary in which droplets flow between the magnetic tweezers. In condition 1, V1 was opened while V2 was closed, syringe (1) was used to generate and store droplets in chip (1), while syringe (2) was used to pump mineral oil in the rest of the circuit. In condition 2, V1 was closed, while V2 was opened, syringe (2) is stopped and the train of droplets were introduced into chip (2), after that condition 1 is reactivated to generate a new train of droplets and so forth. Reprinted with permission from ref. [96]. This work is licensed under a Creative Commons Attribution 4.0 International License. Copyright (2016), Nature

mixing two different cell types in the alginate/NPs solution on-chip, showed that multicelluar spheroids were successfully formed.

A range of biological assays have been performed in magnetic droplets and some displayed cutoff limits that were below the clinical limit. More types of assays can be exploited taking advantage of the high frequency of the generated droplets to screen various assay conditions in a short period of time. Additionally, the majority of assay-based magnetic droplet systems utilize magnetic tweezers because of their advantages such as remote control ability, adjustability of direction and ability to produce large magnitude magnetic forces. It is worth pointing out that despite the variety of detection methods generally used with droplet microfluidics, thus far detection of assays in magnetic droplets has been limited to fluorescence, optical microscopy and SERS techniques. Exploring the applicability of other detection techniques such as electrochemical, chemiluminescence and mass spectrometry can be intriguing to improve the sensitivity of the detection.

Continuous magnetic droplet detection

Thus far, on-chip detection of magnetic materials has been achieved using three miniaturized sensors including GMR [102], superconducting quantum interference devices (SQUID) [103] and Hall sensors [104]. All of these detectors were placed near or integrated into the microfluidic platform to sense the presence of moving magnetic entities with high precision.

The first microfluidic platform for continuous generation and detection of magnetic droplets was developed in 2004 by Pekas et al. [15]. A PDMS platform for continuous monitoring of size, velocity and enumeration of FF droplets included three sets of sensors, each composed of four 20×34 μm spin-valve GMR wired as Wheatstone bridges. In each bridge, two GMRs were used as senseresistors and were positioned in the center below the microfluidic channel, and the other two were used as references. The sealed device was bonded to a printed circuit board that was mounted between the poles of a miniaturized electromagnet that is used to apply an external magnetic field along the 'sense' GMR direction (H_x). Experiments were performed at a magnetic field of 15 Oe, using a model developed by the authors, and $86 \times 13 \times 18$ μm FF droplets with $\chi = 0.25$. The voltage drop at the bridge observed when the front edge of the droplet moved past the GMRs, was used to determine H_x for a moving FF droplet. When the middle of the droplet moved past the sensors, the response slowly decreased and was reversed as the end of the droplet flowed over the sensors. The flow velocity was estimated

from the times between the responses of the two bridges. The distance between the two bridges was 100 μm and the cross-correlation peak position was the time lag between the two signals. The velocity was found to be 19 ± 0.4 mm s^{-1} and the droplet size, estimated as the interval between the two maxima in the GMR signal, was 84 ± 3 μm, which compares to the optically measured size of 86 ± 3 μm. This system has great promise for the continuous detection of moving magnetic droplets.

An on-chip magnetometer based on a planar Hall magnetoresistive (PHR) sensor was fabricated and used to monitor oscillating nL FF droplets [105]. In the sensor, a sensing current was passed between two electrodes positioned parallel to the uniaxial exchange anisotropy field of the trilayer structure (H_{ex}) in the y-direction. The signal profile was determined using electrodes positioned along the x-direction in a magnetic field strength ranging from −30 Oe to +30 Oe applied perpendicular to the current. A stage for the device was located at the center of the magnetic field and a nanovoltmeter (sensitivity 10 nV) was utilized to measure the variation in the voltage arising from the oscillating droplets over the PHR sensor. The magnetization of the moving droplets was measured for both positive and negative z-fields. Using finite element method (FEM) for simulation, the critical droplet length was determined to be 70 μm in order to avoid distortion of the dipole field as the droplet passed over the sensor. The results of this study showed that the sensitivity of the on-chip sensor was influenced by both the sign and magnitude of the applied z-field. As the FF droplet approached the PHR sensor, the voltage profile displayed three distinct changes, which were recorded in terms of a voltage signal (μV) vs. time. As the front edge of the droplet approached the sensor the voltage increased, as the middle of the droplet approached the sensor the signal level dropped to baseline, and finally as the back edge of the droplet approached the sensor the voltage decreased (Fig. 19a–d). A comparison to a conventional VSM showed that the on-chip system required less sample volume. This platform can be used to detect magnetic materials, and monitor magnetic materials on-chip in a continuous flow system.

Supervised discriminant analysis (SDA) was utilized for the first time to discriminate *bivariant* droplets of different: volumes and magnetic contents using a lab-on-a-chip GMR sensor [106]. In the system, a thermally oxidized silicon wafer was used as a substrate and was subjected to a thermal multistep process to produce a 6×100 μm rectangular shape. Using magnetron sputtering, a spin valve stack of SiOx/Ta/Py/CoF/Cu/CoFe/Py/IrMn/Ta was deposited on the substrate. As the droplets pass over the GMR sensor was placed near the channel in which the droplets moved, their local stray magnetic fields were recorded (in volts). The local stray fields were highest at the two edges (front and back) of the droplets, while the width of the detection peak correlated with the length of the droplet. Thus, utilizing the peak width (Δt, ms) and signal amplitude (threshold height, %), the respective size and concentration of the droplet can be determined (i.e. *bivariant*). An algorithm was applied for peak search to filter the recorded signals and determine the thresholds for their width and amplitude. This algorithm was based on the actual number of droplets and the number of droplets obtained by the search to recognize a false rate of counting (FR). For example, at a constant height of 20%, the values of the FR increased either with $\Delta t < 180$ ms or $\Delta t > 300$ ms. Similarly, at a constant Δt (100 ms), FR increased with less than 20% and more than 60% of threshold height. A *bivariant* sample data set comprising the signal amplitude and the peak width was used to perform SDA for the droplets. Two approaches were used to study the quality of the analysis. One (Approach A) was based on Gauss function fitting, which considered the distribution of data in a simple case, while the other (Approach B) was based on calculating a covariance matrix that summarized correlations of the variables. The results showed a 98% success in discriminating FF droplets with differences in volumes as low as 200 pL and concentrations of 2.5 mg/ mL^{-1} that is sufficient for utilization of the system in immune-agglutination assay applications. Additionally, SDA was employed using Approach B to investigate factors affecting discrimination of the droplets. The findings proved that optimization of the flow conditions and signal-to-noise ratio can lead to minimization of the distribution of droplets and their size dispersity, and thereby improve the secreting capability and success rate of SDA for multiplexed assays. Magnetic detection has received relatively small attention because the majority of efforts carried out to date have been devoted to the detection of reactions/assays within droplets rather than determining magnetic functionality. Therefore, combining magnetic detection with other detection techniques should lead to improved selectivities and sensitivities.

Conclusions and outlook

In this review, a comprehensive summary is provided of methods for continuous processing of magnetic droplet in sealed microfluidic devices that have been developed since the time of their inception in 2004. Although many strategies have already been devised for the generation and manipulation of magnetic droplets, and for using these droplets to perform chemical reactions, biological assays and detection, a high potential exists to expand and revolutionize the pool of applications of these platforms. Currently, the primary focus of most investigations is on establishing the proof-of-concept of conventional and existing
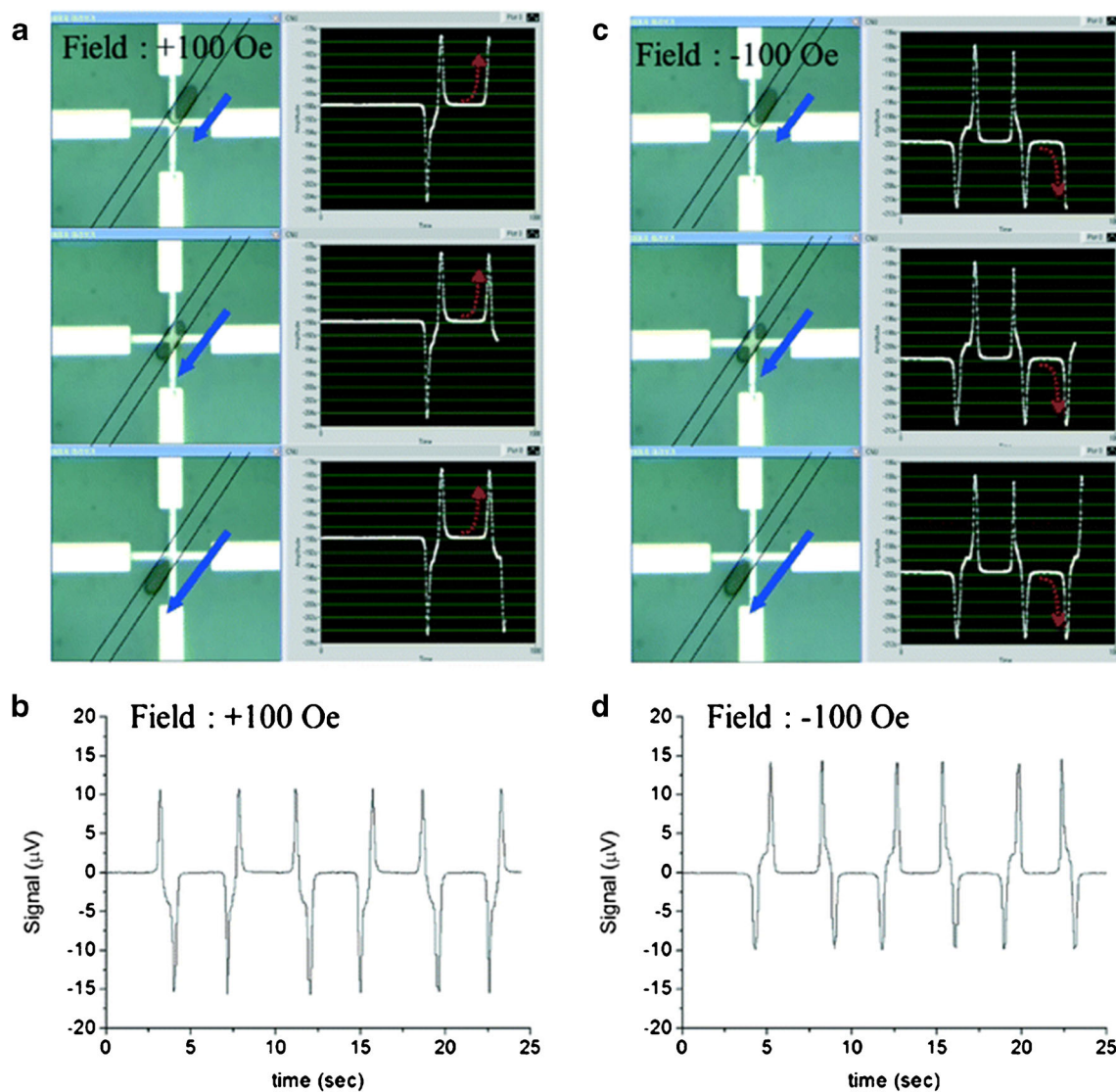
Fig. 19 (a) Microscopic images of forward moving droplet at different positions on the PHR sensor and their measured PHR signals (under +100 Oe applied z-field). (b) The 3 cycles of oscillations of a moving droplet (under +100 Oe applied z-field). (c) Microscopic images of forward moving droplet at various positions on the PHR sensor and their measured PHR signals (under −100 Oe applied z-field). (d) The 3 cycles of oscillations of a moving droplet (under −100 Oe applied z-field). Reprinted with permission from ref. [105]. Copyright (2015), the Royal Society of Chemistry (RSC)

technologies. Thus far, efforts to integrate several droplet reaction and manipulation steps solely using magnetic forces have been successful, however, these systems require that some protocols be performed off-chip prior to or after droplet collection. As a result, it would be beneficial to have the focus of future efforts aimed at developing magnetic lab-on-a-chip platforms be on integrating more steps/components into a single device with a special attention being given to the detection in continuous flow. Advancements in these areas would lead to reductions in analysis time, cost of reagents and carryover and cross contamination. Additionally, it would be significant to explore more applications of these smart droplets including their use in tissue engineering, cell synthesis, drug delivery/screening, cosmetics, enzymatic activity assays and generation of novel and interesting materials.

References

1. Day P, Manz A, Zhang Y (2012) Microdroplet technology: principles and emerging applications in biology and chemistry. Springer Science & Business Media
2. Tice JD, Song H, Lyon AD, Ismagilov RF (2003) Formation of droplets and mixing in multiphase microfluidics at low values of

the Reynolds and the capillary numbers. Langmuir 19(22):9127–9133

3. Tirandazi P, Hidrovo CH (2018) An integrated gas-liquid droplet microfluidic platform for digital sampling and detection of air-borne targets. Sensors Actuators B Chem 267:279–293

4. Tan Y-C, Fisher JS, Lee AI, Cristini V, Lee AP (2004) Design of microfluidic channel geometries for the control of droplet volume, chemical concentration, and sorting. Lab Chip 4(4):292–298

5. Zheng B, Roach LS, Ismagilov RF (2003) Screening of protein crystallization conditions on a microfluidic chip using nanoliter-size droplets. J Am Chem Soc 125(37):11170–11171

6. Li L, Mustafi D, Fu Q, Tereshko V, Chen DL, Tice JD, Ismagilov RF (2006) Nanoliter microfluidic hybrid method for simultaneous screening and optimization validated with crystallization of membrane proteins. Proc Natl Acad Sci 103(51):19243–19248

7. Boedicker JQ, Li L, Kline TR, Ismagilov RF (2008) Detecting bacteria and determining their susceptibility to antibiotics by stochastic confinement in nanoliter droplets using plug-based microfluidics. Lab Chip 8(8):1265–1272

8. Huebner A, Sharma S, Srisa-Art M, Hollfelder F, Edel JB, deMello AJ (2008) Microdroplets: a sea of applications? Lab Chip 8(8):1244–1254

9. Muradoglu M, Stone HA (2005) Mixing in a drop moving through a serpentine channel: a computational study. Phys Fluids 17(7):073305

10. Beer NR, Wheeler EK, Lee-Houghton L, Watkins N, Nasarabadi S, Hebert N, Leung P, Arnold DW, Bailey CG, Colston BW (2008) On-chip single-copy real-time reverse-transcription PCR in isolated picoliter droplets. Anal Chem 80(6):1854–1858

11. Lindsay S, Vázquez T, Egatz-Gómez A, Loyprasert S, Garcia AA, Wang J (2007) Discrete microfluidics with electrochemical detection. Analyst 132(5):412–416

12. Chiu DT, Lorenz RM, Jeffries GDM (2009) Droplets for Ultrasmall-volume analysis. Anal Chem 81(13):5111–5118

13. Baroud CN, Gallaire F, Dangla R (2010) Dynamics of microfluidic droplets. Lab Chip 10(16):2032–2045

14. Gu H, Duits MH, Mugele F (2011) Droplets formation and merging in two-phase flow microfluidics. Int J Mol Sci 12(4):2572–2597

15. Pekas N, Porter MD, Tondra M, Popple A, Jander A (2004) Giant magnetoresistance monitoring of magnetic picodroplets in an integrated microfluidic system. Appl Phys Lett 85(20):4783–4785

16. Scherer C, Figueiredo Neto AM (2005) Ferrofluids: properties and applications. Braz J Phys 35(3A):718–727

17. Nguyen N-T, Ng KM, Huang X (2006) Manipulation of ferrofluid droplets using planar coils. Appl Phys Lett 89(5):052509

18. Al-Hetlani E, Hatt OJ, Vojtíšek M, Tarn MD, Iles A, Pamme N (2010) Sorting and manipulation of magnetic droplets in continuous flow. AIP Conference Proceedings 1311:167–175

19. Lombardi D, Dittrich PS (2011) Droplet microfluidics with magnetic beads: a new tool to investigate drug–protein interactions. Anal Bioanal Chem 399(1):347–352

20. Nguyen N-T (2012) Micro-magnetofluidics: interactions between magnetism and fluid flow on the microscale. Microfluid Nanofluid 12(1–4):1–16

21. Pollack MG, Shenderov AD, Fair R (2002) Electrowetting-based actuation of droplets for integrated microfluidics. Lab Chip 2(2):96–101

22. Baroud CN, de Saint Vincent MR, Delville J-P (2007) An optical toolbox for total control of droplet microfluidics. Lab Chip 7(8):1029–1033

23. Okochi M, Tsuchiya H, Kumazawa F, Shikida M, Honda H (2010) Droplet-based gene expression analysis using a device with magnetic force-based-droplet-handling system. J Biosci Bioeng 109(2):193–197

24. Pamme N (2006) Magnetism and microfluidics. Lab Chip 6(1):24–38

25. Tarn MD, Peyman SA, Robert D, Iles A, Wilhelm C, Pamme N (2009) The importance of particle type selection and temperature control for on-chip free-flow magnetophoresis. J Magn Magn Mater 321(24):4115–4122

26. Lee H, Xu L, Ahn B, Lee K, Oh KW (2012) Continuous-flow in-droplet magnetic particle separation in a droplet-based microfluidic platform. Microfluid Nanofluid 13(4):613–623

27. Tan S-H, Nguyen N-T, Yobas L, Kang TG (2010) Formation and manipulation of ferrofluid droplets at a microfluidic T-junction. J Micromech Microeng 20(4):045004

28. Chen CH, Abate AR, Lee D, Terentjev EM, Weitz DA (2009) Microfluidic assembly of magnetic hydrogel particles with uniformly anisotropic structure. Adv Mater 21(31):3201–3204

29. Huang J-P, Ge X-H, Xu J-H, Luo G-S (2016) Controlled formation and coalescence of paramagnetic ionic liquid droplets under magnetic field in coaxial microfluidic devices. Chem Eng Sci 152:293–300

30. Ohashi T, Kuyama H, Hanafusa N, Togawa Y (2007) A simple device using magnetic transportation for droplet-based PCR. Biomed Microdevices 9(5):695–702

31. Teh S-Y, Lin R, Hung L-H, Lee AP (2008) Droplet microfluidics. Lab Chip 8(2):198–220

32. Yapici MK, Zou J (2008) Permalloy-coated tungsten probe for magnetic manipulation of micro droplets. Microsyst Technol 14(6):881–891

33. Shah GJ, Veale JL, Korin Y, Reed EF, Gritsch HA, Kim C-JC (2010) Specific binding and magnetic concentration of CD 8+ T-lymphocytes on electrowetting-on-dielectric platform. Biomicrofluidics 4(4):044106

34. Gascoyne PRC, Vykoukal JV (2004) Dielectrophoresis-based sample handling in general-purpose programmable diagnostic instruments. Proceedings of the IEEE Institute of Electrical and Electronics Engineers 92(1):22–42

35. Darhuber AA, Valentino JP, Troian SM, Wagner S (2003) Thermocapillary actuation of droplets on chemically patterned surfaces by programmable microheater arrays. J Microelectromech Syst 12(6):873–879

36. Yang C, Zhang Z, Li G (2018) Programmable droplet manipulation by combining a superhydrophobic magnetic film and an electromagnetic pillar array. Sensors Actuators B Chem 262:892–901

37. Guttenberg Z, Muller H, Habermuller H, Geisbauer A, Pipper J, Felbel J, Kielpinski M, Scriba J, Wixforth A (2005) Planar chip device for PCR and hybridization with surface acoustic wave pump. Lab Chip 5(3):308–317

38. Lehmann U, Hadjidj S, Parashar VK, Vandevyver C, Rida A, Gijs MAM (2006) Two-dimensional magnetic manipulation of microdroplets on a chip as a platform for bioanalytical applications. Sensors Actuators B Chem 117(2):457–463

39. Liu J, Tan S-H, Yap YF, Ng MY, Nguyen N-T (2011) Numerical and experimental investigations of the formation process of ferrofluid droplets. Microfluid Nanofluid 11(2):177–187

40. Liu J, Yap YF, Nguyen N-T (2011) Numerical study of the formation process of ferrofluid droplets. Phys Fluids 23(7):072008

41. Ali-Cherif A, Begolo S, Descroix S, Viovy J-L, Malaquin L (2012) Programmable magnetic tweezers and droplet microfluidic device for high-throughput Nanoliter multi-step assays. Angew Chem Int Ed 51(43):10765–10769

42. Sista RS, Eckhardt AE, Srinivasan V, Pollack MG, Palanki S, Pamula VK (2008) Heterogeneous immunoassays using magnetic beads on a digital microfluidic platform. Lab Chip 8(12):2188–2196

43. Baret J-C (2012) Surfactants in droplet-based microfluidics. Lab Chip 12(3):422–433

44. Brouzes E, Kruse T, Kimmerling R, Strey HH (2015) Rapid and continuous magnetic separation in droplet microfluidic devices. Lab Chip 15(3):908–919

45. White AK, VanInsberghe M, Petriv OI, Hamidi M, Sikorski D, Marra MA, Piret J, Aparicio S, Hansen CL (2011) High-throughput microfluidic single-cell RT-qPCR. Proc Natl Acad Sci 108(34):13999–14004

46. Pamme N (2012) On-chip bioanalysis with magnetic particles. Curr Opin Chem Biol 16(3–4):436–443

47. Gijs MA, Lacharme F, Lehmann U (2009) Microfluidic applications of magnetic particles for biological analysis and catalysis. Chem Rev 110(3):1518–1563

48. Chen X, Zhang L (2017) A review on micromixers actuated with magnetic nanomaterials. Microchim Acta 184(10):3639–3649

49. Pamme N, Manz A (2004) On-chip free-flow magnetophoresis: continuous flow separation of magnetic particles and agglomerates. Anal Chem 76(24):7250–7256

50. Link DR, Grasland-Mongrain E, Duri A, Sarrazin F, Cheng Z, Cristobal G, Marquez M, Weitz DA (2006) Electric control of droplets in microfluidic devices. Angew Chem Int Ed 45(16): 2556–2560

51. Schuler F, Schwemmer F, Trotter M, Wadle S, Zengerle R, von Stetten F, Paust N (2015) Centrifugal step emulsification applied for absolute quantification of nucleic acids by digital droplet RPA. Lab Chip 15(13):2759–2766

52. Yan Q, Xuan S, Ruan X, Wu J, Gong X (2015) Magnetically controllable generation of ferrofluid droplets. Microfluid Nanofluid 19(6):1377–1384

53. Ray A, Varma VB, Jayaneel P, Sudharsan N, Wang Z, Ramanujan RV (2017) On demand manipulation of ferrofluid droplets by magnetic fields. Sensors Actuators B Chem 242:760–768

54. Kahkeshani S, Di Carlo D (2016) Drop formation using ferrofluids driven magnetically in a step emulsification device. Lab Chip 16(13):2474–2480

55. Peyman SA, Kwan EY, Margarson O, Iles A, Pamme N (2009) Diamagnetic repulsion—a versatile tool for label-free particle handling in microfluidic devices. J Chromatogr A 1216(52):9055–9062

56. Hartshorne H, Backhouse CJ, Lee WE (2004) Ferrofluid-based microchip pump and valve. Sensors Actuators B Chem 99(2–3): 592–600

57. Alorabi AQ, Tarn MD, Gómez-Pastora J, Bringas E, Ortiz I, Paunov VN, Pamme N (2017) On-chip polyelectrolyte coating onto magnetic droplets–towards continuous flow assembly of drug delivery capsules. Lab Chip 17(22):3785–3795

58. Pamme N, Wilhelm C (2006) Continuous sorting of magnetic cells via on-chip free-flow magnetophoresis. Lab Chip 6(8):974–980

59. Zhang K, Liang Q, Ma S, Mu X, Hu P, Wang Y, Luo G (2009) On-chip manipulation of continuous picoliter-volume superparamagnetic droplets using a magnetic force. Lab Chip 9(20):2992–2999

60. Zhang K, Liang Q, Ai X, Hu P, Wang Y, Luo G (2011) Comprehensive two-dimensional manipulations of picoliter microfluidic droplets sampled from nanoliter samples. Anal Chem 83(20):8029–8034

61. Zhang K, Liang Q, Ai X, Hu P, Wang Y, Luo G (2011) On-demand microfluidic droplet manipulation using hydrophobic ferrofluid as a continuous-phase. Lab Chip 11(7):1271–1275

62. Jo Y, Shen F, Hahn YK, Park J-H, Park J-K (2016) Magnetophoretic sorting of single cell-containing microdroplets. Micromachines 7(4):56

63. Banerjee U, Raj A, Sen A (2018) Dynamics of aqueous ferrofluid droplets at coflowing liquid-liquid interface under a non-uniform magnetic field. Appl Phys Lett 113(14):143702

64. Wu Y, Fu T, Ma Y, Li HZ (2015) Active control of ferrofluid droplet breakup dynamics in a microfluidic T-junction. Microfluid Nanofluid 18(1):19–27

65. Afkhami S, Tyler A, Renardy Y, Renardy M, Pierre TS, Woodward R, Riffle J (2010) Deformation of a hydrophobic ferrofluid droplet suspended in a viscous medium under uniform magnetic fields. J Fluid Mech 663:358–384

66. Li H, Wu Y, Wang X, Zhu C, Fu T, Ma Y (2016) Magnetofluidic control of the breakup of ferrofluid droplets in a microfluidic Y-junction. RSC Adv 6(1):778–785

67. Yamada M, Doi S, Maenaka H, Yasuda M, Seki M (2008) Hydrodynamic control of droplet division in bifurcating microchannel and its application to particle synthesis. J Colloid Interface Sci 321(2):401–407

68. Aboutalebi M, Bijarchi MA, Shafii MB, Hannani SK (2018) Numerical investigation on splitting of ferrofluid microdroplets in T-junctions using an asymmetric magnetic field with proposed correlation. J Magn Magn Mater 447:139–149

69. Sander JS, Erb RM, Denier C, Studart AR (2012) Magnetic transport, mixing and release of cargo with tailored nanoliter droplets. Adv Mater 24(19):2582–2587

70. Misuk V, Mai A, Giannopoulos K, Alobaid F, Epple B, Loewe H (2013) Micro magnetofluidics: droplet manipulation of double emulsions based on paramagnetic ionic liquids. Lab Chip 13(23):4542–4548

71. Chu LY, Utada AS, Shah RK, Kim JW, Weitz DA (2007) Controllable monodisperse multiple emulsions. Angew Chem Int Ed 46(47):8970–8974

72. Adams L, Kodger TE, Kim S-H, Shum HC, Franke T, Weitz DA (2012) Single step emulsification for the generation of multi-component double emulsions. Soft Matter 8(41):10719–10724

73. Nisisako T, Okushima S, Torii T (2005) Controlled formulation of monodisperse double emulsions in a multiple-phase microfluidic system. Soft Matter 1(1):23–27

74. Lin G, Makarov D, Medina-Sánchez M, Guix M, Baraban L, Cuniberti G, Schmidt OG (2015) Magnetofluidic platform for multidimensional magnetic and optical barcoding of droplets. Lab Chip 15(1):216–224

75. Teste B, Jamond N, Ferraro D, Viovy J-L, Malaquin L (2015) Selective handling of droplets in a microfluidic device using magnetic rails. Microfluid Nanofluid 19(1):141–153

76. Varma V, Ray A, Wang Z, Wang Z, Ramanujan R (2016) Droplet merging on a lab-on-a-chip platform by uniform magnetic fields. Sci Rep 6:37671

77. Frenz L, Harrak AE, Pauly M, Bégin-Colin S, Griffiths AD, Baret J-C (2008) Droplet-based microreactors for the synthesis of magnetic Iron oxide Nanoparticles. Angew Chem Int Ed 47(36):6817–6820

78. Paquet C, Jakubek ZJ, Simard B (2012) Superparamagnetic microspheres with controlled macroporosity generated in microfluidic devices. ACS Appl Mater Interfaces 4(9):4934–4941

79. Varma V, Wu R, Wang Z, Ramanujan R (2017) Magnetic Janus particles synthesized using droplet micro-magnetofluidic techniques for protein detection. Lab Chip 17(20):3514–3525

80. Jung JH, Park TJ, Lee SY, Seo TS (2012) Homogeneous biogenic paramagnetic Nanoparticle synthesis based on a microfluidic droplet generator. Angew Chem Int Ed 51(23):5634–5637

81. Ferraro D, Lin Y, Teste B, Talbot D, Malaquin L, Descroix S, Abou-Hassan A (2015) Continuous chemical operations and modifications on magnetic γ-Fe2O3 nanoparticles confined in nanoliter droplets for the assembly of fluorescent and magnetic SiO2@ γ-Fe2O3. Chem Commun 51(95):16904–16907

82. Zhu C, Xu W, Chen L, Zhang W, Xu H, Gu ZZ (2011) Magnetochromatic microcapsule arrays for displays. Adv Funct Mater 21(11):2043–2048

83. Jiang K, Xue C, Arya C, Shao C, George EO, DeVoe DL, Raghavan SR (2011) A new approach to in-situ "micromanufacturing": microfluidic fabrication of magnetic and fluorescent chains using Chitosan microparticles as building blocks. Small 7(17):2470–2476

84. Bokharaei M, Schneider T, Dutz S, Stone RC, Mefford OT, Häfeli UO (2016) Production of monodispersed magnetic polymeric microspheres in a microfluidic chip and 3D simulation. Microfluid Nanofluid 20(1):6

85. Yang C-H, Wang C-Y, Huang K-S, Kung C-P, Chang Y-C, Shaw J-F (2014) Microfluidic one-step synthesis of Fe3O4-chitosan composite particles and their applications. Int J Pharm 463(2): 155–160

86. Cao X, Zang L, Bu Z, Sun L, Guo D, Wang C (2016) Microfluidic fabrication of magnetic porous multi-walled carbon nanotube beads for oil and organic solvent adsorption. J Mater Chem A 4(27):10479–10485

87. Bu Z, Zang L, Zhang Y, Cao X, Sun L, Qin C, Wang C (2017) Magnetic porous graphene/multi-walled carbon nanotube beads from microfluidics: a flexible and robust oil/water separation material. RSC Adv 7(41):25334–25340

88. Lee SW, Choi JS, Cho KY, Yim J-H (2016) Facile fabrication of uniform-sized, magnetic, and electroconductive hybrid microspheres using a microfluidic droplet generator. Eur Polym J 80: 40–47

89. Kaufman G, Montejo KA, Michaut A, Majewski PW, Osuji CO (2017) Photoresponsive and Magnetoresponsive Graphene oxide microcapsules fabricated by droplet microfluidics. ACS Appl Mater Interfaces 9(50):44192–44198

90. Maher S, Santos A, Kumeria T, Kaur G, Lambert M, Forward P, Evdokiou A, Losic D (2017) Multifunctional microspherical magnetic and pH responsive carriers for combination anticancer therapy engineered by droplet-based microfluidics. J Mater Chem B 5(22):4097–4109

91. Shang L, Shangguan F, Cheng Y, Lu J, Xie Z, Zhao Y, Gu Z (2013) Microfluidic generation of magnetoresponsive Janus photonic crystal particles. Nanoscale 5(20):9553–9557

92. Yang Y-T, Wei J, Li X, Wu L-J, Chang Z-Q, Serra CA (2015) A side-by-side capillaries-based microfluidic system for synthesizing size-and morphology-controlled magnetic anisotropy janus beads. Adv Powder Technol 26(1):156–162

93. Lan J, Chen J, Li N, Ji X, Yu M, He Z (2016) Microfluidic generation of magnetic-fluorescent Janus microparticles for biomolecular detection. Talanta 151:126–131

94. Yu X, Zhang C, You S, Liu H, Zhang L, Liu W, Guo S-S, Zhao X-Z (2016) Microfluidic synthesis of multiferroic Janus particles with disk-like compartments. Appl Phys Lett 108(7):073504

95. Hwang DK, Dendukuri D, Doyle PS (2008) Microfluidic-based synthesis of non-spherical magnetic hydrogel microparticles. Lab Chip 8(10):1640–1647

96. Ferraro D, Champ J, Teste B, Serra M, Malaquin L, Viovy J-L, De Cremoux P, Descroix S (2016) Microfluidic platform combining droplets and magnetic tweezers: application to HER2 expression in cancer diagnosis. Sci Rep 6:25540

97. Gao R, Cheng Z, Choo J (2016) Wash-free magnetic immunoassay of the PSA cancer marker using SERS and droplet microfluidics. Lab Chip 16(6):1022–1029

98. Gu S-Q, Zhang Y-X, Zhu Y, Du W-B, Yao B, Fang Q (2011) Multifunctional Picoliter droplet manipulation platform and its application in single cell analysis. Anal Chem 83(19):7570–7576

99. Du W-B, Sun M, Gu S-Q, Zhu Y, Fang Q (2010) Automated microfluidic screening assay platform based on DropLab. Anal Chem 82(23):9941–9947

100. Teste B, Ali-Cherif A, Viovy JL, Malaquin L (2013) A low cost and high throughput magnetic bead-based immuno-agglutination assay in confined droplets. Lab Chip 13(12):2344–2349

101. Yoon S, Kim JA, Lee SH, Kim M, Park TH (2013) Droplet-based microfluidic system to form and separate multicellular spheroids using magnetic nanoparticles. Lab Chip 13(8):1522–1528

102. Millen RL, Kawaguchi T, Granger MC, Porter MD, Tondra M (2005) Giant magnetoresistive sensors and superparamagnetic nanoparticles: a chip-scale detection strategy for immunosorbent assays. Anal Chem 77(20):6581–6587

103. Shinji K, Takao Y, Ken H, Akira M, Saburo T (2001) Development of a new detection method for DNA molecules. Supercond Sci Technol 14(12):1131

104. Ejsing L, Hansen MF, Menon AK, Ferreira H, Graham D, Freitas P (2004) Planar hall effect sensor for magnetic micro-and nanobead detection. Appl Phys Lett 84(23):4729–4731

105. Kim KW, Reddy V, Torati SR, Hu XH, Sandhu A, Kim CG (2015) On-chip magnetometer for characterization of superparamagnetic nanoparticles. Lab Chip 15(3):696–703

106. Lin G, Fomin VM, Makarov D, Schmidt OG (2015) Supervised discriminant analysis for droplet micro-magnetofluidics. Microfluid Nanofluid 19(2):457–464

107. Habault D, Dery A, Leng J, Lecommandoux S, Meins JFL, Sandre O (2013) Droplet microfluidics to prepare magnetic polymer vesicles and to confine the heat in magnetic hyperthermia. IEEE Trans Magn 49(1):182–190. https://doi.org/10.1109/tmag.2012.2221688

108. Dietzel A (2016) Microsystems for pharmatechnology. Springer

109. Toepke MW, Beebe DJ (2006) PDMS absorption of small molecules and consequences in microfluidic applications. Lab Chip 6(12):1484–1486

110. Tian W-C, Finehout E (2009) Microfluidics for biological applications, vol 16. Springer Science & Business Media,

111. Tsao C-W (2016) Polymer microfluidics: simple, low-cost fabrication process bridging academic lab research to commercialized production. Micromachines 7(12):225

112. Griffin S (2003) Fused-silica capillary-the story behind the technology. LC GC EUROPE 16(5):276–289

113. Ren K, Dai W, Zhou J, Su J, Wu H (2011) Whole-Teflon microfluidic chips. Proc Natl Acad Sci 108(20):8162–8166